

Alma Mater Studiorum Università di Bologna
Archivio istituzionale della ricerca

Hydrological factors affecting rainfall-induced shallow landslides: From the field monitoring to a simplified slope stability analysis

This is the final peer-reviewed author's accepted manuscript (postprint) of the following publication:

Published Version:

Bordoni, M., Meisina, C., Valentino, R., Lu, N., Bittelli, M., Chersich, S. (2015). Hydrological factors affecting rainfall-induced shallow landslides: From the field monitoring to a simplified slope stability analysis. ENGINEERING GEOLOGY, 193, 19-37 [10.1016/j.enggeo.2015.04.006].

Availability:

This version is available at: <https://hdl.handle.net/11585/472967> since: 2015-09-08

Published:

DOI: <http://doi.org/10.1016/j.enggeo.2015.04.006>

Terms of use:

Some rights reserved. The terms and conditions for the reuse of this version of the manuscript are specified in the publishing policy. For all terms of use and more information see the publisher's website.

This item was downloaded from IRIS Università di Bologna (<https://cris.unibo.it/>).
When citing, please refer to the published version.

(Article begins on next page)

Accepted Manuscript

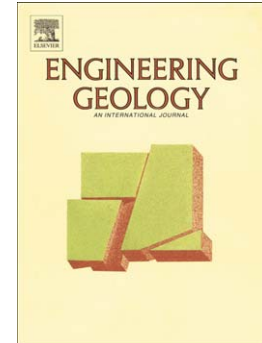
Hydrological factors affecting rainfall-induced shallow landslides: from the field monitoring to a simplified slope stability analysis

M. Bordoni, C. Meisina, R. Valentino, N. Lu, M. Bittelli, S. Chersich

PII: S0013-7952(15)00122-2
DOI: doi: [10.1016/j.enggeo.2015.04.006](https://doi.org/10.1016/j.enggeo.2015.04.006)
Reference: ENGEO 4014

To appear in: *Engineering Geology*

Received date: 16 November 2014
Revised date: 9 February 2015
Accepted date: 8 April 2015



Please cite this article as: Bordoni, M., Meisina, C., Valentino, R., Lu, N., Bittelli, M., Chersich, S., Hydrological factors affecting rainfall-induced shallow landslides: from the field monitoring to a simplified slope stability analysis, *Engineering Geology* (2015), doi: [10.1016/j.enggeo.2015.04.006](https://doi.org/10.1016/j.enggeo.2015.04.006)

This is a PDF file of an unedited manuscript that has been accepted for publication. As a service to our customers we are providing this early version of the manuscript. The manuscript will undergo copyediting, typesetting, and review of the resulting proof before it is published in its final form. Please note that during the production process errors may be discovered which could affect the content, and all legal disclaimers that apply to the journal pertain.

Hydrological factors affecting rainfall-induced shallow landslides: from the field monitoring to a simplified slope stability analysis

M. Bordoni ^a, C. Meisina ^a, R. Valentino ^b, N. Lu ^c, M. Bittelli ^d, S. Chersich ^a

^a Department of Earth and Environmental Sciences, University of Pavia, Via Ferrata 1, 27100 Pavia
- Italy

^b Department of Civil and Environmental Engineering and Architecture, University of Parma, Viale
G.P. Usberti 181/A, 43100 Parma – Italy

^c Department of Civil & Environmental Engineering, Colorado School of Mines, 1500 Illinois
Street, 80401 Golden - CO, USA

^d Department of Agricultural Sciences, University of Bologna, Viale Fanin 44, 40127 Bologna -
Italy

Corresponding author: Massimiliano Bordoni - mail:
massimiliano.bordoni01@universitadipavia.it - Via Ferrata 1, 27100 Pavia - Italy -
telephone: +39 0382 985840 - fax: +39 0382 985890

Abstract

Rainfall-induced shallow landslides can seriously affect cultivations and infrastructures and cause human losses. A continuous monitoring of unsaturated soils hydrological properties is needed to understand the effects of pore water pressure and water content on shallow landslides triggering and slope safety factor. In this work, the impact of water content, pore water pressure and hydrological hysteresis on safety factor reconstruction is analyzed by applying two different models (Lu and

Godt's and SLIP models) to a monitored slope located in Oltrepò Pavese (Northern Italy). A shallow landslide event in the studied slope during the monitoring allowed for identifying the triggering mechanism and modeling the safety factor changes. The conditions of instability mechanism develop in periods with frequent rainfalls: the uprising of a perched water table in the soil profile gets nil or positive pore water pressure, which, linked with the nil effective soil cohesion of some soil horizons, allows for the shallow landslides triggering. The safety factor trends correctly predicted unstable conditions (safety factor ≤ 1.0) in correspondence of the shallow landslide triggering time on the basis of both water content and pore water pressure. A better prediction gets when the safety factor is modeled considering the hysteresis effects. Modeling the safety factor on the basis of water content can make a good assessment of shallow failures triggering conditions only for failures in unsaturated soils and for completely saturated soils. Instead, considering pore water pressure it is possible estimating safety factor changes linked with the development of positive pore water pressures, which can be linked in some cases to shallow landslides development.

Keywords: shallow landslides; safety factor; water content; pore water pressure; hysteresis

1. Introduction

Rainfall-induced shallow landslides affecting superficial deposits of small thickness (generally lower than 2 m) are common phenomena all over the world. In the last years, important events were recorded in many regions of Italy (Cascini et al., 2008; Montrasio and Valentino, 2008; Damiano et al., 2012; Cevasco et al., 2013; D'Amato Avanzi et al., 2013; Sorbino and Nicotera, 2013; Zizioli et al., 2013, 2014; Grelle et al., 2014), in Switzerland (Von Ruetten et al., 2011; Lehmann and Or, 2012; Springman et al., 2013), in Hong Kong (Fuchu et al., 1999), in South Korea (Park et al., 2013), in USA (Schmidt et al., 2001; Godt et al., 2008a, b; Godt et al., 2009; Baum et al., 2010), in many areas of Central America (Capra et al., 2003; Harp et al., 2009; Eichenberg et al., 2013).

Shallow landslides are generally triggered by very intense rainfall events (Howard et al., 1988; Montrasio and Valentino, 2008). Although they involve small volumes of soils, as a consequence of particularly intense and concentrated rainfall, they can be densely distributed across territories (Zizioli et al., 2013) and, moreover, can affect slopes close to urbanized areas. For this reason, they can have bad effects on cultivations, infrastructures and, sometimes, human losses.

Before the triggering event, shallow soils of the affected slopes are usually unsaturated. Many authors identified the quick increase in pore water pressure and the development of positive pore pressures, due to the formation of a perched water table, as the most important cause for shallow landslides triggering (Lim et al., 1996; Vanapalli et al., 1996; Godt et al., 2008a, 2008b 2009; Baum et al. 2010; Lu and Godt, 2013).

One of the most widespread methods to predict shallow landslides triggering is represented by rainfall thresholds, which represent the rainfall amount, determined on the basis of analysis of past phenomena, that, when reached or exceeded, are likely to trigger landslides (Reichenbach et al.,

1998). In particular, rainfall thresholds based on rainfall intensity- duration relationships, have been defined in many different climatic and geological settings (Caine, 1980; Cancelli and Nova, 1985; Reichenbach et al., 1998; Guzzetti et al., 2008; Martelloni et al., 2012). Moreover, real-time rainfall data compared with rainfall thresholds have been incorporated into landslide warning systems, as in San Francisco Bay region in USA (Wilson and Wieczorek, 1995), Malaysia (Lee et al., 2009), Emilia Romagna Region in Italy (Martelloni et al., 2012).

Another approach for the prediction of rainfall-induced shallow landslides is linked with a continuous monitoring of hydrological and mechanical properties of the soil. Recent studies focusing on monitoring of slopes susceptible to shallow landslides (Lim et al., 1996; Simoni et al., 2004; Matsushi et al., 2006; Matsushi and Matsukura, 2007; Godt et al., 2008a, 2008b 2009; Baum et al. 2010; Bittelli et al., 2012; Damiano et al., 2012; Leung and Ng, 2013; Smethurst et al., 2012; Springman et al., 2013) demonstrated how monitoring techniques allow to identify the soil hydrological and mechanical conditions during shallow landslides triggering and some fundamental properties that are essential to characterize and model landslides development.

Soil water content and pore water pressure are the basic soil features to be considered in the stability analysis of a slope during a rainfall event. In fact, soil water content and pore water pressure data from continuous monitoring of unsaturated soils have been revealed very useful to be implemented in different kinds of stability models, such as closed-form equations based on a limit equilibrium analysis (Lu and Godt, 2008, 2013), physically based models (Campbell, 1975; Montgomery and Dietrich, 1994; Iverson, 2000; Baum et al., 2002, 2008; Montrasio and Valentino, 2008), and Finite Element Models (FEM) (Cuomo and Della Sala, 2013; Springman et al., 2013). In all these situations, it is required an accurate knowledge of the constitutive relationships which identify the main soil hydrological properties. In particular, the Soil Water Characteristic Curve (SWCC), which relates the pore water pressure and the water content, allows for the

characterization of hydrological and also mechanical behavior of usually unsaturated soils (Lu et al. 2013). Moreover, the hysteretic nature of SWCC (Topp and Miller, 1966; Mualem, 1976; Parlange, 1976; Kool and Parker, 1987; Lu and Likos, 2006; Fredlund et al., 2011; Likos et al., 2013; Lu et al., 2013), linked to *in-situ* processes due to different drying and wetting cycles the soils suffer in natural conditions, determines the development of a main drying curve (MDC) and a main wetting curve (MWC), thus it can have practical implications on water movements in soil and on the mechanical behavior of unsaturated soils in terms of deformation and shear strength (Wheeler et al., 2003; Likos et al., 2013).

In the most of models for rainfall-induced shallow landslides triggering conditions, only drying path parameters are considered and the hysteretic effects are generally neglected (Montgomery and Dietrich, 1994; Iverson, 2000; Baum et al., 2002, 2008; Bathurst et al., 2005; Askarinejad et al., 2012; Park et al., 2013). On the other hand it is worth noting that the topsoil is under wetting process during rainfall infiltration, therefore neglecting the wetting path could affect the assessment of rainfall-induced shallow landslides triggering mechanisms (Ebel et al., 2010; Tsai, 2010; Ma et al., 2012; Likos et al., 2013).

The main objectives of the present work can be summarized as follows: 1) to identify the main hydrological behaviors of the topsoil based on field monitoring of a test-site slope, focusing on the conditions which can lead to the shallow failures; 2) to evaluate the effect of the topsoil hydrological properties on modeling the safety factor at slope scale; 3) to investigate the effect of hydrological hysteresis on the estimation of the time trend of the safety factor on the basis of field measurements; 4) to compare the time trends of the safety factor of the studied slope by applying different simplified slope stability models based on the limit equilibrium method.

2. Material and methods

2.1 *The study slope*

2.1.1 *Geological and climatic settings*

The test-site slope is located in the north-eastern part of Oltrepò Pavese (Northern Italy), a hilly region corresponding to the northern termination of Apennines (Fig. 1). In this area the bedrock is characterized by a Mio-Pliocenic succession that is called "Serie del Margine" (Vercesi and Scagni, 1984), constituted of continental deposits (sand, sandstones and conglomerates) overlying marine (especially marls) and evaporitic (chalky marls, gypsum) deposits (Fig. 1). The bedrock strata mainly dip east-northeast with moderate inclinations. Shallow soils which derive from the bedrock weathering have prevalently a clayey silt or a silty sand texture and thickness which ranges between a few centimeters to 2.5 m (Zizioli et al., 2013).

In correspondence of the studied slope, the bedrock is made up of gravel, sand and poorly cemented conglomerates with a low percentage of marls (Rocca Ticozzi Conglomerates) and presents an upper weathered part (Fig. 1, 2). Superficial soils, derived by bedrock weathering, are prevalently clayey-sandy silts and clayey-silty sands with different amount of pebbles and carbonate concretions. Their thickness, determined through trench pits and micro boreholes, increases from the top to the bottom of the slope, from few centimeters till 1.85 m also due to the presence of landslides accumulation areas (Fig. 2, 3).

The studied slope has features that can be considered typical of the surrounding area. Hillslopes are characterized by medium-high topographic gradient ranging from 22 to 35°. In particular, slope angle values around 30° are present along the test-site slope section in correspondence of the monitoring station, except for some pre-existing shallow landslides source areas (Fig. 3).

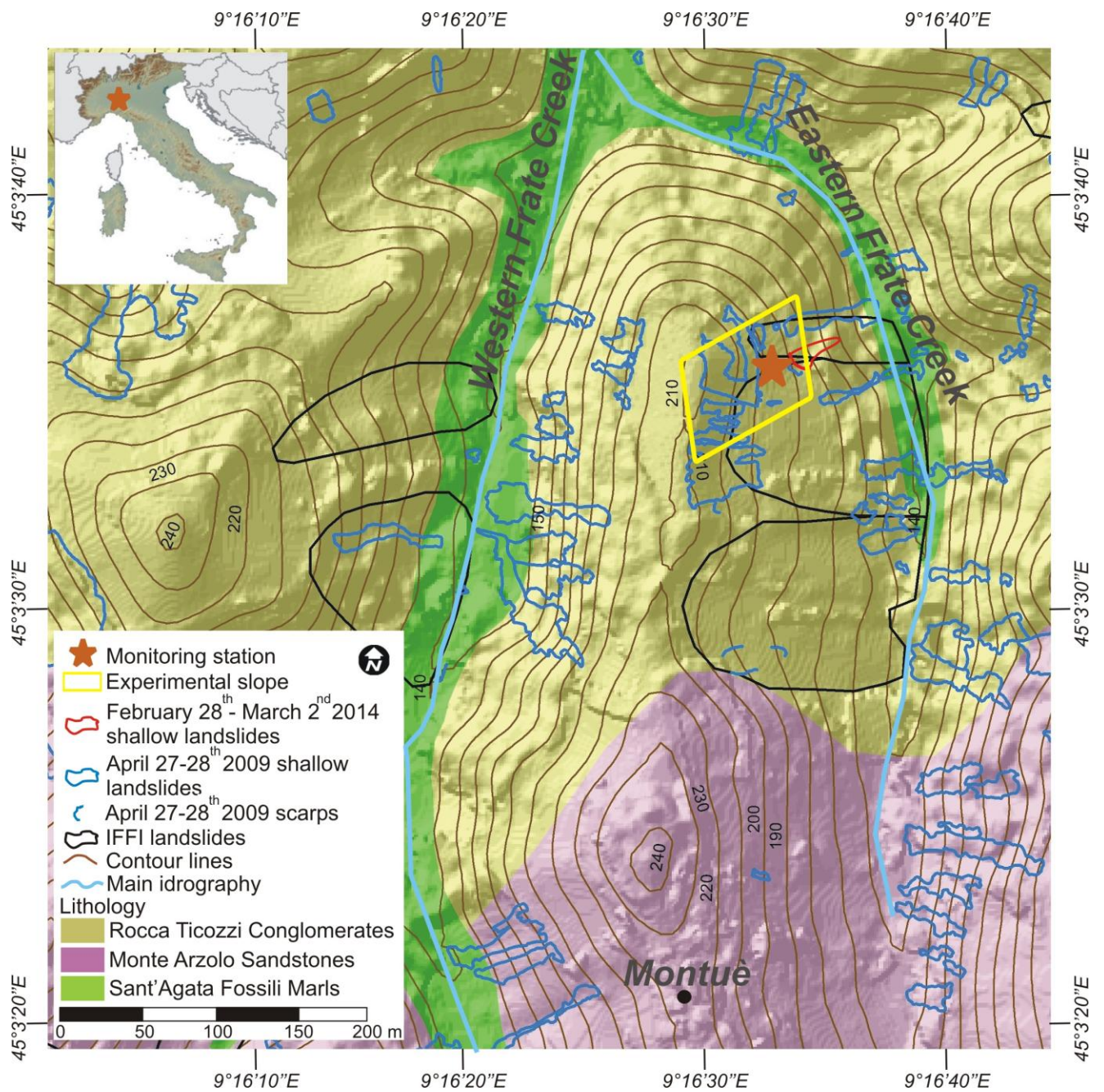


Figure 1. Location of the monitored experimental slope and geological sketch map of the surrounding area.

Furthermore, the East-facing slope descends towards a rather small and narrow valley formed by a creek (Eastern Frate Creek). The slope elevation ranges from 210 to 170 m a.s.l. and the monitoring station is located at 185 m.a.s.l. The land use is mainly constituted by grass and shrubs passing to a

woodland of black robust (*Robinia Pseudoacacia*) trees at the bottom of the slope, where some vineyards had been abandoned since the eighties of the last century. Roots of living vegetation are present from the ground level till about 0.3-0.4 m in depth.

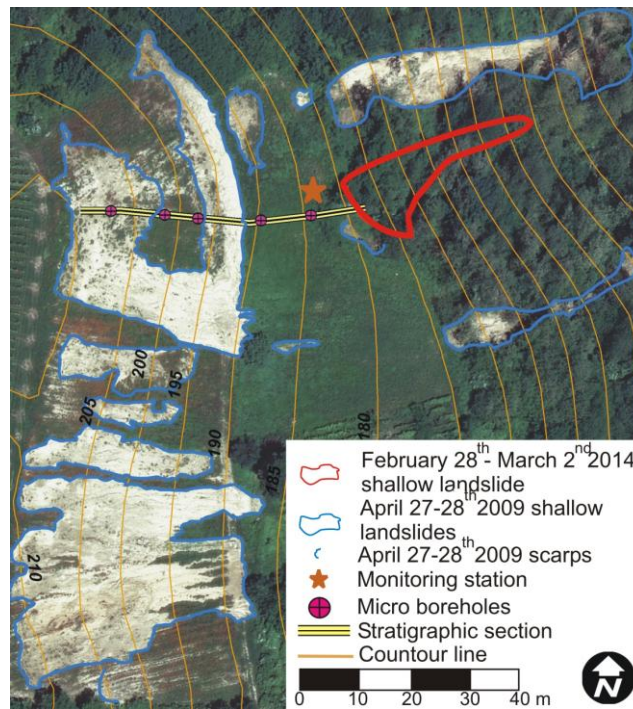


Figure 2. Detailed view of the test-site slope where the monitoring station was installed. The aerial photograph of the area was taken by Ditta Rossi s.r.l. (Brescia, Italy) in May 18th 2009.

The area of Oltrepò Pavese has a continental climatic regime. Considering recent rainfall data available from 2004 to 2014 coming from a weather station located closely near the study area at a similar elevation (Canevino rain-gauge station, ARPA Lombardia monitoring network), it is possible to note a general decreasing in the yearly cumulated rainfall with respect to the mean annual rainfall measured in the period 1921-1979 (Rossetti and Ottone, 1979), from 775.2 mm to 684.4 mm (Fig. 4a).

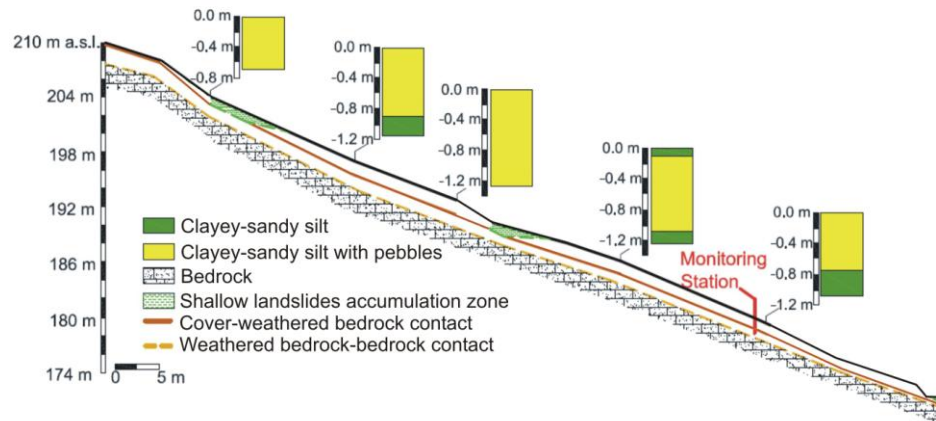


Figure 3. Stratigraphic section along the test-site slope (the track of the section and the pits locations are indicated in Fig. 2).

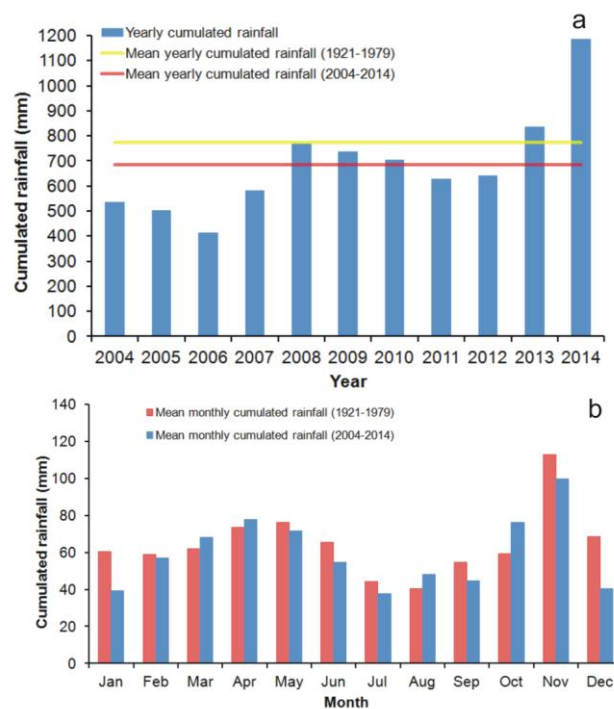


Figure 4. Mean yearly (a) and mean monthly (b) rainfall amount for the periods 1921-1979 and 2004-2014 measured at Canevino rain-gauge station.

The maximum rainfall amount is in November and the minimum one is in July (Fig. 4b).

2.1.2 Landslides distribution

The area where the study slope is located is characterized by a high density of past landslides.

In the test-site slope, near by the monitoring station, the Italian Landslides Inventory (IFFI) database indicates the presence of three rotational slides (Cruden and Varnes, 1996) with deep failure surfaces (Fig. 1). These phenomena, as other similar deep landslides of the Oltrepò Pavese hillslopes, were triggered by prolonged rainfalls and can be considered currently dormant.

As shown in Fig. 4a, in the last five years the yearly rainfall amounts in the study area have always had values higher than the mean yearly amount of the period 2004-2013. In this time span, in Oltrepò Pavese, many shallow landslides events occurred, affecting superficial soils above the weathered or not-weathered bedrock and with a failure surface located in correspondence of the interface between topsoil and bedrock, at a depth ranging between 0.5 and 2.0 m from ground, and, more rarely, above this limit, in correspondence of the contact between soil levels with different permeability.

The triggering event of 27th and 28th April 2009 was the most important of the last five years and the first documented case of rainfall induced shallow landslides that hit the north-eastern sector of Oltrepò Pavese since the fifties of the last century. Shallow landslides occurred on April 2009 were triggered in consequence of an extreme rainfall event characterized by 160 mm of cumulated rain in 62 h (20% of the yearly average amount of 1921-1979 period, 25% of the yearly average amount of 2004-2013 period) with a maximum intensity of 22 mm/h at 9 p.m. on 27th April (Zizioli et al., 2013). In the surrounding area of about 240 km² this event caused more than 1600 shallow

landslides, with the highest density (29 landslides per km²) registered in the zone where the monitored slope is located.

During the April 2009 event, the test-site slope was affected by many rainfall-induced shallow landslides (Fig. 2), whose source areas tended to be concentrated in correspondence of slope angle changes (Fig. 2, 3) and had failure surfaces located at a depth ranging between 0.5 and 1.0 m from ground level (Fig. 3).

Further shallow landslides occurred in this area: a) in the period between March and April 2013, due to close rainfall events which determined an high cumulated rainfall amount (till 227.8 mm measured in Canevino rain gauge, equal to 28.5% of the annual average amount; Zizioli et al., 2014); b) between 28th February and 2nd March 2014, due to an intense rainfall event (68.9 mm in 42 h registered by the rain gauge of the monitoring station installed in the test-site slope) following thirty rainy days with a cumulated rainfall amount of 105.5 mm.

While no phenomena were observed in the study slope due to the 2013 rainfall events, a shallow landslide was triggered during the 28th February-2nd March 2014 event 15 m far from the monitoring station (Fig. 1, 2), near the bottom of the slope, very close to a little scarp occurred in April 2009. The source area of the shallow landslide occurred on 2nd March 2014 has the same slope angle of the zone where the monitoring station is located (30°), and the failure surface is at 1.0 m from ground level.

2.2 Study slope soil characterization

2.2.1 Pedological description and characterization

A multidisciplinary study was carried out to characterize the superficial soils and the weathered bedrock of the study slope.

In correspondence of the monitoring station, a pedological description of the representative soil profile was performed. Seven main soil horizons were identified (Fig. 5): an OL horizon (0-0.01 m), labeled as A; an A1 horizon (0.01-0.1 m), labeled as B; an Ak2 horizon (0.1-0.2 m), labeled as C; an Apgk3 horizon (0.2-0.4 m), labeled as D; a Bgk horizon (0.4-0.7 m), labeled as E; a BCgk horizon (0.7-1.1 m), labeled as F; a Cgk horizon (1.1-1.3 m), labeled as G. The weathered bedrock (We. Bedr.), composed by sand and poorly cemented conglomerates, was identified at 1.3 m from ground level, in agreement with the soil thickness measured near the monitoring station (Fig. 3).

According to the IUSS Working Group WRB (2007) the soil is classified as Calcic Gleysol. All the soil horizons have a silty texture, except for the G horizon that has a silty-clayey texture. Different amounts of secondary carbonate accumulations such as soft coatings were identified in the profile.

Calcimetry analyses provided an indication of the total carbonate content at different depths. This parameter is rather uniform both in the soil profile and in the weathered bedrock ranging from 13.7 to 16.1 % (Fig. 5a), except for the G level where the carbonate content is much higher than the other levels, reaching values till 35.3 % at 1.2 m from ground (Fig. 5a). Level G can be then considered as a calcic horizon and the less permeable level of the entire soil profile, as already shown in similar pedological profiles having a calcic horizon at least 0.2 m thick (Stakman and Bishay, 1976; Baumhardt and Lascano, 1993). Pedological characterization also shows that the soil has an organic carbon (O.C.) content lower than 3.0 %, that decreases with depth (Fig. 5b), and a rather steady basic pH (8.3-8.8) along the profile. Moreover, also the cationic exchange capacity (C.E.C.) keeps rather steady along the soil profile, with values ranging between 12.3 and 15.9 meq/100 g (Fig. 5c).

Below 0.2 m from the surface in the soil profile, redoximorphic features have been recognized, testifying an episaturation of water and a movement of perched water table that, in case of extreme rainfall events, could rise till the more superficial soil horizons causing the complete saturation of the soil profile.

2.2.2 Mineralogical and geotechnical characterization

An X-Ray diffraction analysis on *tout-venant* from different soil levels confirmed the abundance of carbonate (Carbonate min.) and clay minerals (Clay min.) all along the soil profile (Fig. 5d). Instead, in the weathered bedrock, there is a prevalence of feldspar minerals (Feld. min.; Fig. 5d) due to its sandy and conglomeratic character.

On the basis of the grain-size distribution, soil horizons have a high silty content, ranging from 51.1% to 65.6%, that tends to slightly grow with depth, and clay content higher than 21.3% (Fig. 5e; Tab. 1). Sand and gravel contents are always low in the soil levels, till 0.5 and 7.5 % in the G horizon, respectively. Instead, the weathered bedrock at 1.4 m, immediately below the topsoil, is constituted by a sand lens, as testified by a sand content of 75.0% (Fig. 5e; Tab. 1).

By analyzing the clay soil fraction ($< 2 \mu\text{m}$), it mostly appears constituted by smectite and chlorite (Fig. 5e). In particular, smectite constitutes about 50% of the soil finest fraction, and then, about 10-15% of the solid particles of the studied soils.

According to USCS classification, soil horizons are prevalently non plastic or slightly plastic soils (CL). Liquid limit (w_L) ranges from 38.5 to 41.9 %, while plastic limit (w_P) ranges from 24.2 to 25.3 % and both keep steady along depth (Fig. 5g). Plasticity index (P_I) follows the trend shown by w_L and w_P (Tab. 1).

The unit weight (γ) and porosity for both the topsoil and the weathered bedrock were determined from undisturbed samples. Unit weight has a significant increase in the F horizon from 16.7 to 18.6 kN/m^3 and then keeps rather steady with depth (Fig. 5h; Tab. 1). Instead, in correspondence of the same level, the porosity shows an important decrease, passing from 49.8 to 42.3 % (Fig. 5i; Tab. 1).

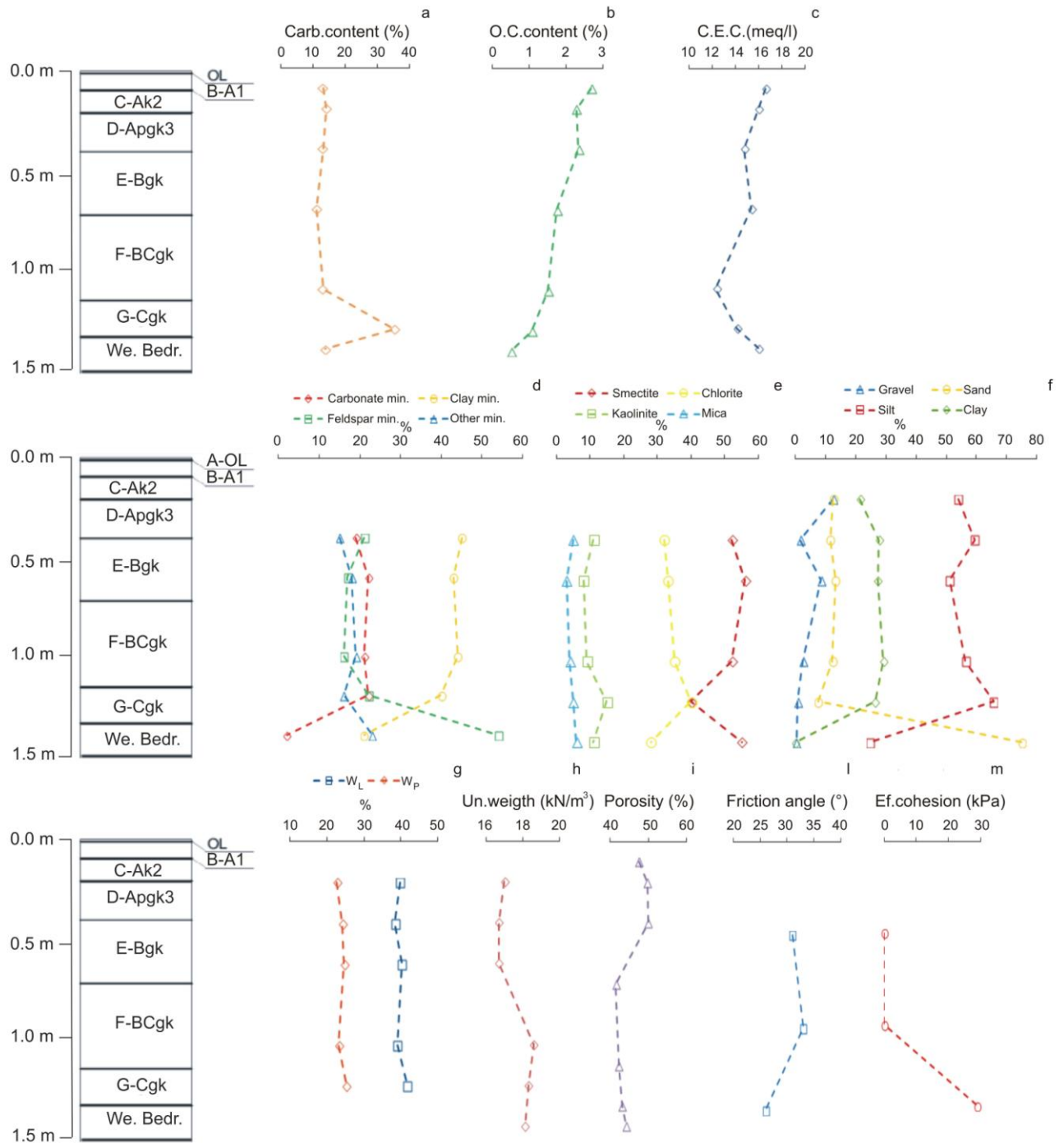


Figure 5. Test site representative soil profile and weathered bedrock pedological classification and selected properties trend along depth: a) carbonate content; b) organic carbon content; c) cationic exchange capacity; d) mineral content; e) grain size distribution; f) mineral content of soil fraction < 2 μ m; g) liquid and plastic limits; h) unit weight; i) porosity; l) friction angle; m) effective cohesion.

	Representative depth m	Gravel %	Sand %	Silt %	Clay %	w _L %	P _I %	γ kN/m ³	φ' °	c' kPa
C	0.2	12.33	12.50	53.92	21.25	39.79	17.18	17.00		
D	0.4	1.50	11.40	59.42	27.68	38.46	14.25	16.70		
E	0.6	8.47	13.23	51.10	27.20	40.32	15.65	16.70	31	0
F	1.0	2.40	12.20	56.40	29.00	39.15	15.94	18.60	33	0
G	1.2	0.50	7.50	65.63	26.37	41.85	16.54	18.25	26	29
We. Bedr.	1.4	0.20	75.00	24.80	0.00	-	-	18.06		

Table 1. Selected geotechnical and physical features of the studied slope soil and weathered bedrock.

On the basis of these features, the soil profile can be divided into two main sectors: the first shallow sector, which includes the topsoil, extends till 0.7 m from the ground level, while the second deeper sector extends below and is more compact than the upper one, as testified by the higher unit weight and the lower porosity.

Peak shear strength parameters were reconstructed for the E, F and G horizons through triaxial tests (Fig. 5l, m; Tab. 1). E and F horizons have friction angle (ϕ') between 31° and 33° and nil effective cohesion (c'). The G horizon is characterized by a friction angle equal to 26° and effective cohesion of 29 kPa.

Oedometer tests were performed for undisturbed samples taken in correspondence of both the E horizon (0.40-0.55 m from ground), the F horizon (0.85-1.0 m from ground) and the G horizon (1.2 m from ground). All these soil horizons are over-consolidated. Furthermore, similar values of compressibility index (around 0.2) and swelling index (around 0.05) were measured in these horizons.

2.3 The monitoring equipment

The integrated field monitoring station installed in the test-site slope (Fig. 6) consists in a rain gauge (Model 52203, Young Comp., Traverse City, MI), a thermo-hygrometer (Model HMP155A, Campbell Sci. Inc., Logan, UT), a barometer (Model CS100, Campbell Sci. Inc., Logan, UT), an anemometer (Model WINDSONIC, Campbell Sci. Inc., Logan, UT) and a net radiometer (Model NR-LITE 2, Kipp & Zonen, Delft, Netherlands). These meteorological sensors are linked to six Time Domain Reflectometer (TDR) probes (Model CS610, Campbell Sci. Inc., Logan, UT) equipped with a multiplexer (SDMX50, Campbell Sci. Inc., Logan, UT), installed at 0.2, 0.4, 0.6, 1.0, 1.2, 1.4 m from ground level to measure the soil water content (Fig. 5). TDR measurements of water content were checked in the first stages of the monitoring and, in order to reject uncorrected values, an appropriate algorithm was applied.

Moreover, a combination of three tensiometers (Model Jet-Fill 2725, Soilmoisture Equipment Corp., Santa Barbara, CA) and three Heat Dissipation (HD) sensors (Model HD229, Campbell Sci., Logan, UT), installed at 0.2, 0.6, 1.2 m from ground level in different soil horizons, are used to measure pore water pressure. The tensiometers directly measure the pore water pressure, while the HD sensors use the Flint et al. (2002) equation to convert in pore water pressure the measured change in soil temperature after a constant heating period. HD sensors allow to acquire only pore water pressure lower than -10^1 kPa (Bittelli et al., 2012); thus, tensiometers are installed in correspondence of the HD sensors to measure values higher than -10^1 kPa.

As well as for the TDR probes, the depths of the installation of HD sensors and of tensiometers were chosen on the basis of the soil stratigraphy under the monitoring station and for evaluating the responses of unsaturated zone at different depths in terms of water content and pore water pressure in relation with different meteorological conditions.

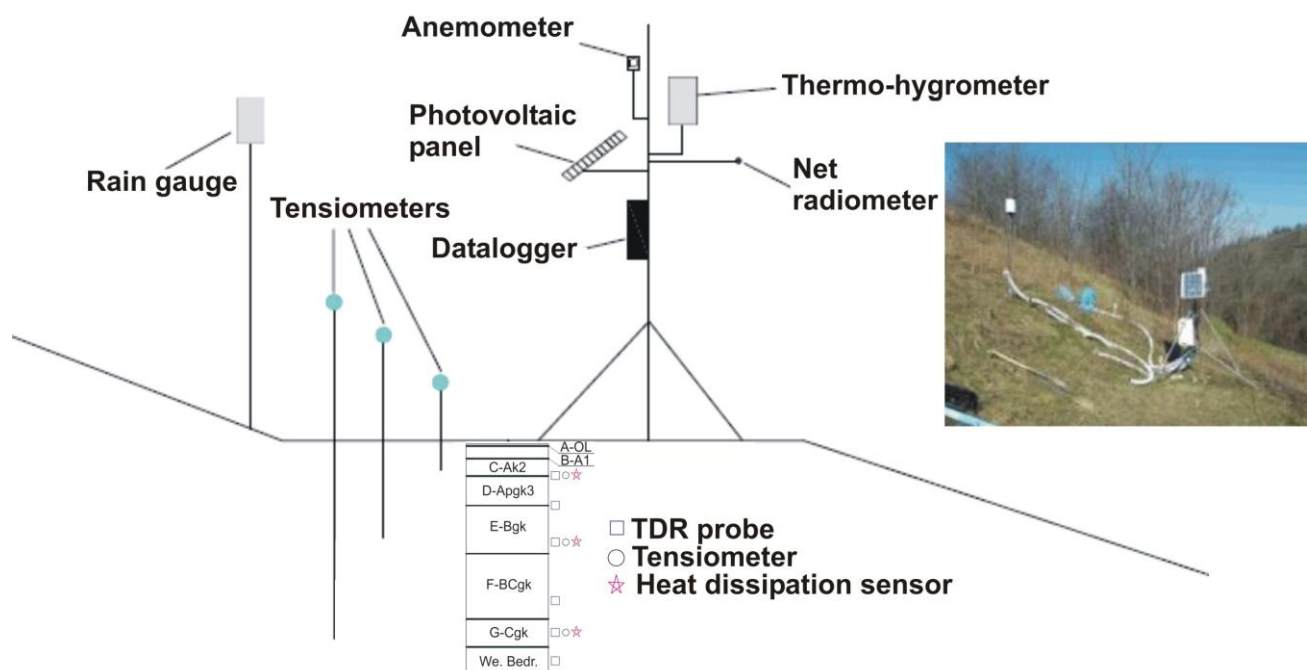


Figure 6. Schematic representation of the monitoring station.

The measurement devices were positioned in undisturbed soil layers next to a trench pit purposely dug for their installation and were connected to the datalogging system. TDR probes, HD sensors and tensiometers were installed behind the trench pit and the datalogging system to keep them in natural undisturbed soil. In this way, the water flows have been kept in natural conditions and the presence of preferential flows can be negligible. The meteorological sensors were installed in correspondence of the datalogging system, except for the rain gauge, which was positioned on the ground next to the trench pit.

The field data are collected by a CR1000X datalogger (Campbell Sci. Inc.) powered by a photovoltaic panel. In this work, field data acquired during a continuous monitoring of about two years (27th March 2012-17th April 2014) are analyzed.

2.4 Models for slope stability analysis

At the moment, different models could be used for the stability analysis of a slope potentially affected by rainfall-induced shallow landslides in unsaturated conditions. They can be roughly distinguished into numerical and simplified methods. Numerical methods allow a detailed study of the problem at the slope scale, by considering complex constitutive models for the partially saturated soil and steady-state seepage in both saturated and unsaturated conditions. Nevertheless, the computational load is relatively high and determining the values of the parameters is often very hard. If the study is aimed at evaluating the stability conditions of a class of slopes on a wide area, the safety factor of a single slope can represent a useful concise parameter, especially if the final objective is a “distributed” stability analysis on large areas. From this viewpoint, two “simplified” models based on the limit equilibrium method have been chosen in the present study. Although the selected models have been only applied at slope scale, the further goal of the validation process is the possible extension of the same models at local and regional scale.

In a simplified model the values of hydrological parameters as pore water pressure or water content are used to take into account the soil unsaturated conditions on safety factor computation (Duncan and Wright, 2005). The Lu and Godt's (2008) model was selected because, through the term of suction stress, which allows for representing the mechanical behaviour of an unsaturated soil (Lu and Likos, 2004), the safety factor can be calculated alternatively by considering water content or pore water pressure. For this reason, by using the same model, the main differences on computations deriving from choosing one or the other parameter can be highlighted. Furthermore, the equations of the suction stress proposed by Lu et al. (2010) allow for considering the SWCCs parameters on suction stress computation. In this way it was possible analyzing the effect of the hysteresis on suction stress and, then, on the safety factor, by considering either the MDCs or the MWCs parameters.

The safety factor trends estimated through the Lu and Godt's model were compared with that one reconstructed by applying a different simplified model (SLIP model) which is based on a scheme of computation only linked to the seasonal trend of the soil water content.

The hydrological data collected by the monitoring station allowed for identifying the studied soil hydrological behaviours and for reconstructing field hysteretic SWCCs, whose parameters were used in the safety factor estimation through the Lu and Godt's model. Furthermore, these data were inserted in two hydrological softwares (HYDRUS-1d and RETC) for modelling the studied soil Hydraulic Conductivity Functions (HCFs) so determining the soil saturated hydraulic conductivity K_s . The SWCCs and HCFs properties were employed in HYDRUS-1d code to model the trends in time of pore water pressure and water content and compare them with the measured ones at different depths. In this way the reliability of the reconstructed soil properties was confirmed, and, then, the modelled trends of hydrological parameters at some depths were coupled with those measured by the monitoring station trends as fundamental inputs to evaluate the change in safety factor in time and to identify the triggering conditions of slope failures.

2.4.1 Lu and Godt's model

Lu and Godt (2008) developed a closed-form equation to extend the infinite slope model for the evaluation of the safety factor under partially saturated conditions, also to evaluate the trend of the safety factor in relation to the changes in the soil hydrological parameters linked with rainfall infiltration.

Into the typical equation expressing the limit equilibrium method applied to an infinite slope, they inserted the equation of the generalized effective stresses σ' (Eq. 1) that also takes into account partially saturated conditions (Lu and Likos, 2004):

$$\sigma' = (\sigma - u_a) - \sigma^s \quad \text{Eq. 1}$$

where σ is the total stress, u_a is the pore air pressure and σ^s is the suction stress, which groups all the inter-particle physico-chemical forces and inter-particle capillary forces which counterbalance the shear stress in unsaturated soils (Lu and Likos, 2006). When a soil approaches saturation, the suction stress is reduced, and this phenomenon can be assumed as the main triggering mechanism for landslides (Lu et al., 2010).

Lu and Likos (2006) demonstrated as suction stress depends on the soil water content θ , through the term of degree of saturation S_e , and on the soil pore water pressure $u_a - u_w$ (Eq. 2):

$$\sigma^s = -(u_a - u_w) S_e \quad \text{Eq. 2}$$

in which the saturation degree is computed through Eq. 3:

$$S_e = \frac{\theta - \theta_r}{\theta_s - \theta_r} \quad \text{Eq. 3}$$

where θ is the soil water content, and θ_s and θ_r are the saturated and the residual water content, respectively.

Lu et al. (2010) proposed two formulations for calculating suction stress only considering either the saturation degree (Eq. 4) or the pore water pressure (Eq. 5):

$$\sigma^s = -\frac{S_e}{\alpha} \left(S_e^{\frac{n}{1-n}} - 1 \right)^{\frac{1}{n}} \quad \text{Eq. 4}$$

;

$$\sigma^s = \begin{cases} -\frac{(u_a - u_w)}{\left(1 + (\alpha(u_a - u_w))^n\right)^{\frac{n-1}{n}}} & (u_a - u_w) > 0 \\ (u_a - u_w) & (u_a - u_w) \leq 0 \end{cases} \quad \text{Eq. 5}$$

In Eqs. 4 and 5, the terms α and n represent the fitting parameters of Van Genuchten's (1980) equation, which, together with θ_s and θ_r , allow for the characterization of soil hydrological properties through the SWCC.

Lu and Godt's (2008) model for slope stability analysis uses the term of suction stress σ^s to calculate the safety factor (F_s) considering the change on soil hydro-mechanical properties linked to rainfall infiltration (Eq. 6):

$$F_s = \frac{c' + (\gamma z \cos^2 \beta - \sigma^s) \tan \varphi'}{\gamma z \sin \beta \cos \beta} \quad \text{Eq. 6}$$

where c' is the effective cohesion, γ is the unit weight of the soil, z is the depth below ground level in which a potential sliding surface could develop, β is the slope angle and φ' is the friction angle. Considering stress variations in vertical directions and a steady vertical seepage, Eq. 6 can be rearranged to Eq. 7:

$$F_s = \frac{\tan \varphi'}{\tan \beta} + \frac{2c'}{\gamma z \sin 2\beta} - \frac{\sigma^s}{\gamma z} [(\tan \beta + \cot \beta) \tan \varphi'] \quad \text{Eq. 7}$$

Due to the different formulations which can be used for σ^s calculation, F_s can be modelled since on the basis of either soil water content or soil pore water pressure data.

2.4.2 SLIP model

The SLIP model (Montrasio, 2000; Montrasio and Valentino, 2008; Montrasio et al., 2011, 2012) is a physically based model for the analysis of triggering time of rainfall-induced shallow landslides. The model assumes that the potential failure surface is located, with respect to the ground level, at a depth H corresponding to the contact between two soil layers with different permeability, where the base layer is less permeable than the upper one. The model considers the potentially unstable topsoil has homogeneous and characterized by isotropic features in terms of hydrological and geotechnical properties.

The model defines the safety factor F_s by applying the limit equilibrium method to an equivalent infinite slope that is composed of two soil parts: a partially saturated part and another that represents the saturated zones. Homogenization is used to obtain the downgraded (with respect to the original conditions) shear strength characteristics of an equivalent soil that is stable in the presence of both saturated and partially saturated zones; this is consistent with both the principles of soil mechanics and the application of the limit equilibrium method.

For simplicity, the saturated zones are represented in the model by a saturated sub-layer of thickness mH ($0 < m < 1$). The saturated sub-layer mH co-exists with an unsaturated sub-layer of thickness $H(1-m)$ and, in its turn, the parameter mH is related to the total amount of rainwater.

The sliding process begins when a relatively wide continuous stratum of saturated soil (mH) has formed, usually in correspondence of the contact between levels with different permeability. The stability of a slope is evaluated through the safety factor (F_s), by also taking into account the partial saturation contribution to the soil shear strength, in terms of the apparent soil cohesion, for soil under partially saturated conditions. F_s is then calculated as follows (Eq. 8):

$$F_s = \frac{\cot \beta \tan \phi' [\Gamma + m(p_a - 1)] + c' \Omega}{\Gamma + mp_a} \quad \text{Eq. 8}$$

where

$$\Gamma = G_s(1-p) + pS_e \quad \text{Eq. 9}$$

$$p_a = p(1-S_e) \quad \text{Eq. 10}$$

$$\Omega = \frac{2}{\sin 2\beta H \gamma_w} \quad \text{Eq. 11}$$

$$C' = [c' + c_\psi] \Delta S = [c' + AS_e(1-S_e)^\lambda (1-m)^{\alpha'}] \Delta S \quad \text{Eq. 12}$$

$$m = \frac{\xi}{pH(1-S_e)} \sum_{i=1}^{\varpi} h_i \exp[-K_T(t-t_i)] \quad \text{Eq. 13}$$

The symbols from Eq. 8 to Eq. 13 have the following meanings: β is the slope angle; φ' is the soil friction angle; γ_w is the unit weight of the water; H is the thickness of the potentially unstable layer; ΔS is the unit length of the soil slice; m represents the saturated fraction of the soil layer with respect to its thickness H ; p is the porosity of the soil; p_a is the amount of the soil porosity occupied by the air; G_s is the specific weight of the soil; S_e is the saturation degree of the soil; c' is the effective soil cohesion; c_ψ is the apparent cohesion given by the partial saturation of the soil; A , λ and α' are numerical calibration parameters; ξ is a runoff coefficient; K_T is the discharge capacity of the slope; t is the current time instant; and t_i is the time to which the rainfall depth h_i corresponds.

As shown by Eq. 8, the SLIP model assumes that F_s is directly correlated with the rainfall amount during a particular event by considering the factor m as a function, at each considered time step, of previous rainfalls and of the parameter K_T , which is linked to the drainage coefficient of the soil. Furthermore, F_s depends on the soil saturation degree S_e and, then, by the soil water content according to Eq. 3.

3. Results

3.1 Monitored soil hydrological parameters dynamics

The monitoring station data were used to determine the dynamics of water content and pore water pressure in both the soil profile and the weathered bedrock (Fig. 7). Average hourly values of water content and pore water pressure were considered. Due to break of the tensiometer at 0.2 m from ground level, at this depth pore water pressure in the range between 0 and -10^1 kPa was not measured since November 2012 till the end of the analyzed period. No data were acquired between January 10th and 15th 2014 due to a not correct functioning of the station alimentation system.

In the analyzed period, the water content ranged between 0.10 and $0.45 \text{ m}^3 \cdot \text{m}^{-3}$ in the topsoil, and between 0.15 and $0.38 \text{ m}^3 \cdot \text{m}^{-3}$ in the weathered bedrock. Instead, pore water pressure ranged from positive values, till 12.7 kPa in the G horizon, to values in the order of -10^3 kPa.

The field pore water pressure measurements had a good level of confidence in a range close to saturation till around -300 kPa. In fact, some laboratory tests (filter paper test) and field tests (measures with portable tensiometer, Model Quick Draw, Soilmoisture Equipment Corp.) performed in different seasons gave pore water pressure values very similar to those measured by the monitoring system, with differences in the order of 1-2 kPa, very close to saturation, till 10 kPa far from saturated conditions.

The installed tensiometers require a correction of the measured values due to height of the water present in the column of the instrument, with an increase of 1 kPa of the initial values for each 0.1 m of depth in the soil. For this reason, it is possible to measure also positive values of the pore water pressure, as already shown in previous works (Zhan et al., 2006). Furthermore, the upper limit of pore water pressure measurements is limited by height of the water in the column of the instrument (Zhan et al., 2006) and it reaches values in the order of 6 kPa in the E horizon and 12 kPa in the G horizon.

It is immediately clear that water content and pore water pressure dynamics are strictly connected to rainfall trends and that different hydrological behaviours can be identified in the soil profile (Fig. 7).

The soil horizons till 0.6-0.7 m from ground level had quick response than the deepest soil horizons to long dry or long wet periods. In summer months, decreases of the water content and of the pore water pressure are faster in the most shallow soil horizons than in the deeper ones (Fig. 7), due to evapotranspiration effects and to the water uptake from the roots of grass and shrubs. During rather prolonged rainy periods following dry periods, as in autumn months, re-wetting of the shallowest soil horizons is fast (Fig. 7, 8a, b), as well as after rainfall events characterized by low duration and low cumulative rainfall (e.g. 34.8 mm in 21 h on 31st October - 1st November 2012, Fig. 7a, b; 42.2 mm in 34 h on 6th-7th October 2013, Fig. 6a, b). On the other hand, only prolonged rainy periods, with many rainfall events in few days or weeks, can provoke an increase of the pore water pressure and of the water content in correspondence of soil horizons deeper than 0.6-0.7 m and of weathered bedrock (Fig. 7).

In autumn re-wetting events, the wetting front reached a depth of 0.4 m from ground in about 12-15 h since the rain start, and similarly reached a depth of 0.6 m in about 20-22 h (Fig. 8a, b). In these cases, superficial soil levels did not get completely saturation and the pore water pressure increased from -400 kPa only till about -100 kPa in correspondence of the E horizon. The wetting front seemed stopped in correspondence of the contact between the E and F horizons. At this level, due to the lower porosity and the higher depth of the soil beneath 0.6-0.7 m from ground, the wetting front slows and is not able to propagate at further depths given the restricted rainfall duration, and then only prolonged rainy periods can cause a re-wetting in deepest soil horizons.

The rapid re-wetting as consequence of early autumn rainfalls of the soil horizons till 0.6-0.7 m from ground may also be due to the presence of desiccation cracks and other macro-voids all along

the soil profile, where preferentially rainwater could flow. This fact could promote a quick development towards near saturated conditions of the cracks and the macro-voids (Bittelli et al., 2012; Smethurst et al., 2012).

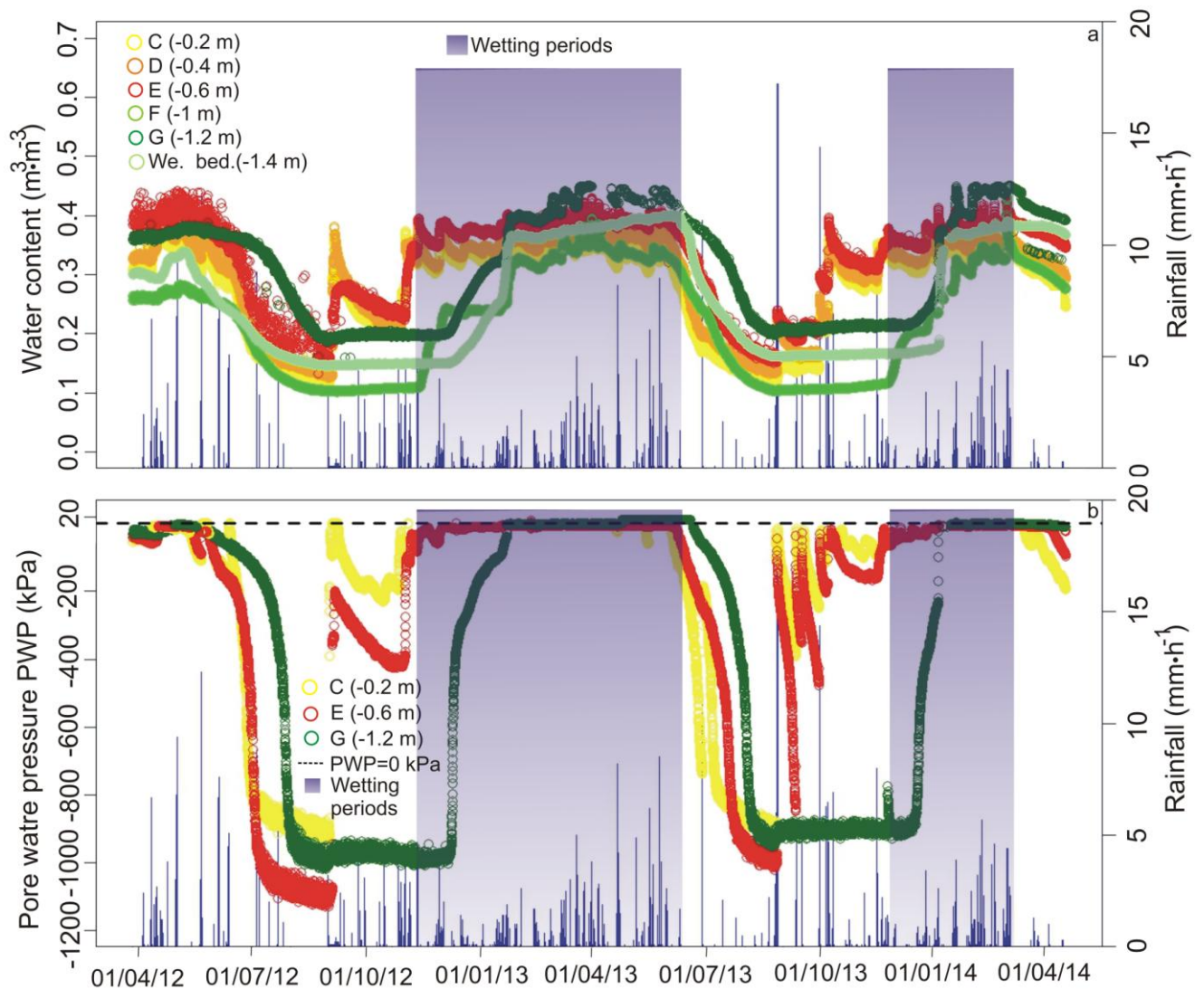


Figure 7. Water content (a) and pore water pressure (b) dynamics in relation with rainfalls for the analyzed time span.

This behaviour seems more pronounced during concentrated and moderately intense summer rainstorms, such those occurred on 27th June 2013 (13.3 mm in 2 h), on 26th August 2013 (16.5 mm in 3 h; Fig. 8e, f), and on 11th September 2013 (9.1 mm in 3 h).

These particular phenomena seem linked to non-equilibrium processes due to a fast infiltration phase (Rogers and Klute, 1971; Ross and Smettem, 2000; Simunek et al., 2003; Vogel et al., 2010; Diamantopoulos et al., 2012), in which, during a drainage or an infiltration process, pore water pressure or water content trend lags behind each other by the SWCC equilibrium. Furthermore, TDR probes seem to be not able to identify the quick transfer of the wetting front in cracks and in the macro-voids in superficial horizons after summer concentrated rainfalls. Instead, it could not be possible to completely monitor the non-equilibrium processes during summer events because the HD sensors in the shallow soil levels (till 0.6 m from ground) were not able to measure pore water pressure values during and immediately after the rainfall event intensity peak. For this reason the pore water pressure trends for C and E horizons appeared not continuous (Fig. 8f).

In winter and spring months, especially between December and May, frequent precipitations can increase the soil wetness till it approaches or reaches saturated conditions. In particular, completely saturated conditions were reached in the G horizon during wet periods in winter and spring 2013 and 2014, as testified by the values of pore water pressure which kept quite steady around 0 kPa till reaching positive values around 1-3 kPa in correspondence of more intense rainfall events (e.g. 29.8 mm in 24 h in 24-25th March 2013, Fig. 8c, d; 24.6 mm in 15 h in 30th March 2013; 29.5 mm in 26 h in 4-5th April 2013; 34.6 mm in 47 h in 18-19th January 2014; 68.9 mm in 42 h 28th February - 2nd March 2014; Fig. 8g, h).

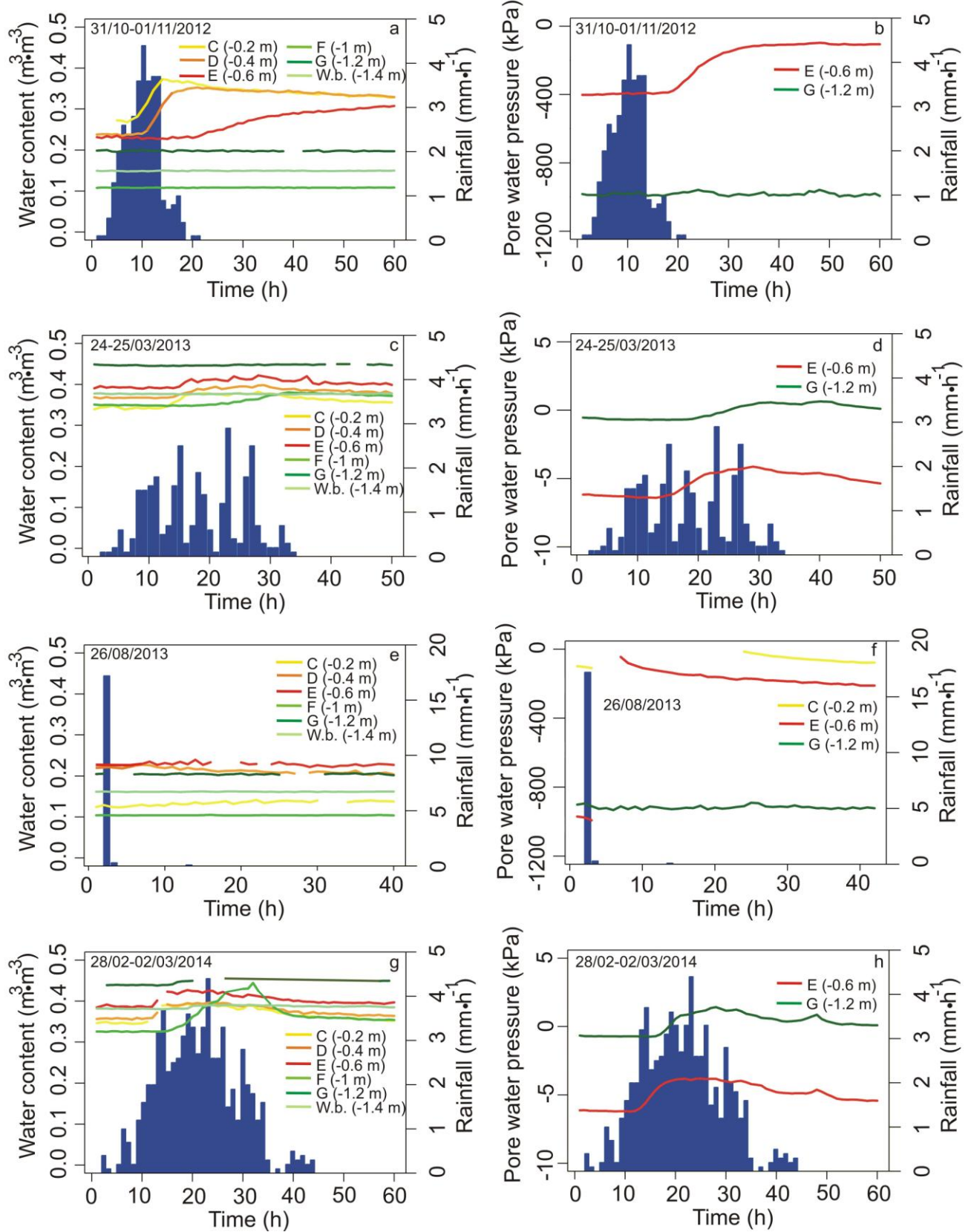


Figure 8. Water content and pore water pressure trends in soil and weathered bedrock levels during and immediately after different rainfall events: 31st October - 1st November 2012 water content (a)

and pore water pressure (b) trends; 24-25th March 2013 water content (c) and pore water pressure (d) trends; 26th August 2013 water content (e) and pore water pressure (f) trends; 28th February - 2nd March 2014 water content (g) and pore water pressure (h) trends.

Moreover, rather prolonged rainy periods with many rainfall events could cause another pore water pressure increase, as that occurred in the end of April-first day of May 2013, when pore water pressure reached 12.7 kPa in the G horizon (Fig. 7b). When the pore water pressure in the G level ranged from -2 kPa to positive values for many days, the TDR probe of this level measured anomalous values of soil water content around $0.45 \text{ m}^3 \cdot \text{m}^{-3}$, i.e. a value higher than the porosity of this soil.

In the E horizon, in wet periods, the pore water pressure did not reach positive values, but it only increased till values of -3 kPa, thus testifying that this soil level approached saturated conditions, also in agreement with the highest values of soil water content measured by the TDR probe at the same depth (around $0.40 \text{ m}^3 \cdot \text{m}^{-3}$). It is possible that non-equilibrium processes can also develop in this situation.

Ross and Smettem (2000) and Voget et al. (2010) demonstrated that during fast infiltration phases water content and pore water pressure can lag between their equilibrium and the soil water content can increase till saturated values, while pore water pressure keeps quite steady. This could explain the presence of a quite steady negative pore water pressure even when the soil water content is close to saturation.

In correspondence of rainfall events occurred during wetting periods, the infiltrated rainwater reached soil levels till 0.6 m from ground in about 12-14 h, which is faster than the arrival time for autumn re-wetting events, due to the higher initial soil water content (Fig. 8). After rainfall

occurrence in wetting periods, the wetting front is also able to reach a deeper level in the soil profile: in particular, it reaches 1.0 m from ground in about 20-22 h (Fig. 8c, g) and 1.2 m from ground (in the G horizon) in about 25 h (Fig. 8d, h). Then, the wetting front spends about 12 h to cover the first 0.6 m of the soil profile and about 18 h to reach the further 0.6 m. The higher time required for the infiltrated rainwater to reach both the F and the G horizon confirms that these levels are less permeable than the most superficial ones.

During wetting periods, water content in the weathered bedrock was lower than the overlying G horizon (Fig. 7a).

According to the monitored data, it could be supposed that during these periods a perched water table formed in the G horizon. This level, which is less permeable due to the higher content in carbonates, is the first to reach complete saturation during prolonged rainy periods or after very intense rainfall events, while the upper soil levels could be saturated later, through a mechanism similar to a perched water table rising (Li et al., 2013).

In particular, this uprising was observed in correspondence of 28th February - 2nd March 2014 and it probably was the main cause which determined the shallow landslide triggering near the monitoring station (Fig. 8g, h). In correspondence of this event, the topsoil till 0.6-0.7 m from ground level and the G horizon behaved as during other rainfall events in winter-spring months and in other wetting periods, as shown in Fig. 8c, d. On the contrary, the F horizon, which is positioned immediately above the G level, was affected by a significant increase of the water content, passing from 0.32 m³·m⁻³ to values similar of those measured in the G horizon (Fig. 8g). This increase testified an uprising of the perched water table, which is usually present in the G horizon in wetting periods till 0.8-1.0 m, leading to the complete saturation of the F horizon as well. This condition was already noticed in previous works (Tohari et al., 2007) and can be considered the triggering mechanism of rainfall-induced shallow landslides in the test-site slope.

3.2 Field reconstruction of SWCCs

For the soils belonging to the C, E and G horizons, where both the TDR probes, the tensiometers and the HD sensors were installed, SWCCs were reconstructed by coupling field measurements of pore water pressure and water content (Fig. 9). The values measured during drying or wetting periods of the monitored time span, also shown in Fig. 7, were distinguished.

SWCCs are usually reconstructed for the estimation of the unsaturated soil hydromechanical properties (Fredlund et al., 2011). Unsaturated conditions are represented by the negative range of pore water pressure, till 0 kPa. For this reason, in these reconstructions, positive values of pore water pressure measured in the G horizon have been disregarded.

It was noticed how an hydrological hysteresis process affected the investigated soils. A Main Drying Curve (MDC) and a Main Wetting Curve can be identified (MWC) for both the E and the G horizons, with a not-closed hysteretic behavior (Fig. 9) and, as a consequence, a complete hysteresis cycle passing from drying to wetting conditions can be noticed (Fig. 9). SWCC of the E horizon showed a high degree of scattering, especially in conditions very close to saturation (Fig. 9b), due to very short hysteresis processes occurred after more intense rainfall events during drying and wetting phases, which determine numerous less evolved scanning drying and wetting curves. Instead, SWCC of the G horizon shows less scattered field measured values (Fig. 9c), because, due to its higher depth in the soil profile, this horizon is not affected by single rainfall events but only by more prolonged rainy or dry periods.

As before mentioned, for the C horizon, only a MDC is evident, due to the lack of tensiometric measurements during wetting periods (Fig 9a).

In correspondence of pore water pressure values around -10^3 kPa, the trend of each MDC on logarithmic scale shows a very high gradient. This effect is linked to the main drying phase of the studied soil during the dry season, when pore water pressure keeps rather steady and water content, instead, slowly and continuously decreases (Fig. 7).

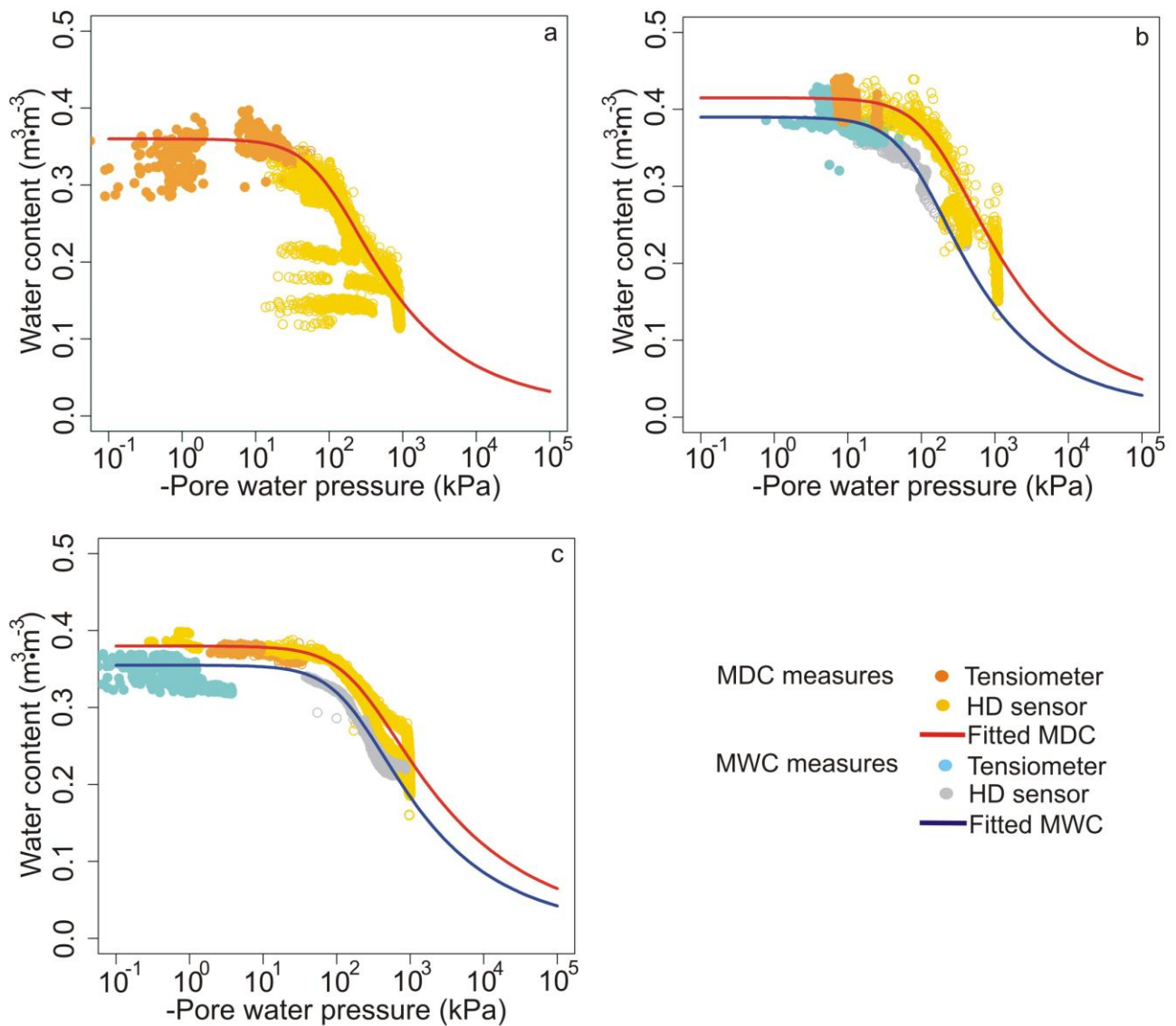


Figure 9. Field reconstructed complete SWCCs for the C (a), E (b) and G (c) horizons at the monitoring station.

Field measured data have been interpolated by using the Van Genuchten's (1980) equation, whose fitting parameters were evaluated through the Marquardt's (1963) algorithm. The reliability of the fitting procedure has then evaluated by considering the Root Mean Square Error (RMSE) statistical index. RMSE values of the fitted field curves ranged between 0.0092 and 0.0165 $\text{m}^3 \cdot \text{m}^{-3}$, thus testifying that there is a good agreement with field experimental data, especially for the G horizon, where the effect of short hysteresis processes is less pronounced (Tab. 2).

	MDC					MWC				
	α_d kPa^{-1}	n_d -	θ_{sd} $\text{m}^3 \cdot \text{m}^{-3}$	θ_{rd} $\text{m}^3 \cdot \text{m}^{-3}$	RMSE $\text{m}^3 \cdot \text{m}^{-3}$	α_w kPa^{-1}	n_w -	θ_{sw} $\text{m}^3 \cdot \text{m}^{-3}$	θ_{rw} $\text{m}^3 \cdot \text{m}^{-3}$	RMSE $\text{m}^3 \cdot \text{m}^{-3}$
C	0.016	1.30	0.370	0.01	0.0159	-	-	-	-	-
E	0.007	1.35	0.425	0.01	0.0165	0.010	1.43	0.395	0.01	0.0104
G	0.004	1.20	0.390	0.01	0.0092	0.006	1.26	0.370	0.01	0.0103

Table 2. Van Genuchten equation fitting parameters of field fitted MDCs and MWCs for the studied soil horizons.

Due to the not-closed global hysteresis loop for E and G horizons (Fig. 9b, c), θ_s decreased from 0.425 $\text{m}^3 \cdot \text{m}^{-3}$ to 0.395 $\text{m}^3 \cdot \text{m}^{-3}$ for the E horizon and from 0.39 $\text{m}^3 \cdot \text{m}^{-3}$ to 0.37 $\text{m}^3 \cdot \text{m}^{-3}$ for the G horizon (Tab. 2), in the order of about 7-8 % between drying and wetting paths. For field SWCCs of the E and G horizons, passing from drying to wetting conditions, an increase in the α_w fitting parameter is highlighted with respect to the α_d (Tab. 2), as already shown in previous works (Kool and Parker, 1987; Likos et al., 2013). Furthermore, due to not-closed hysteretic behavior of the soils, also the n_w parameter increases with respect to n_d (Tab. 2). Instead, θ_{rd} and θ_{rw} coincide in the field MDCs and MWCs for both E and G horizons (Tab. 2).

3.3 Modeled soil hydraulic conductivity functions

The HYDRUS-1D code Vers. 4.16 (Simunek et al., 2008, Simunek et al., 2013) and RETC code Vers. 6.xx (Van Genuchten et al., 1991) have been used to perform an inverse modeling of the Hydraulic Conductivity Functions (HCFs) of the C, E and G horizons based on the field measured water contents and pore water pressures (Fig. 10). The Hydraulic Conductivity Functions have been fitted by using the Mualem (1976)-Van Genuchten (1980) model. The HCF of a soil is characterized by the same fitting parameters of the corresponding SWCC (Lu et al. 2013). For this reason, the fitting parameters of the HCFs modelled through HYDRUS-1D were compared with the parameters of field reconstructed SWCCs to further evaluate their reliability.

It has been noticed that the Van Genuchten fitting parameters estimated with the HYDRUS-1D code are substantially equal to the corresponding parameters of the field reconstructed SWCCs (Tab. 2). Only parameters α_d and α_w of the E and G horizons present a little difference, with values slightly lower (respectively, 0.005 than 0.007 kPa⁻¹ and 0.009 than 0.010 kPa⁻¹ for E horizon, 0.002 than 0.004 kPa⁻¹ and 0.004 than 0.006 kPa⁻¹ for G horizon) than the ones reported in Tab. 2. For this reason, the field estimated MDC and MWC properties are in good agreement with the field data and can be employed in the slope stability analysis.

The modelling of HCFs based on field data through HYDRUS-1d and RETC also allowed for estimating the saturated hydraulic conductivity K_s corresponding to a pore water pressure of 0 kPa. Modeled HCFs of both the E and G horizons show not-closed hysteretic loops, while for the C horizon only the MDC path of the HCF was estimated, due to the lack of data needed to fit also the MWC path (Fig. 10). Equal values of the drying saturated hydraulic conductivity K_{sd} have been obtained for the C and E horizons (7.2 cm/h), while the G horizon has a K_{sd} value equal to 3.0 cm/h, which is lower than that of the overlying soil levels (Tab. 3). It has been noticed that modeled K_{sd} values of the investigated soils are higher than 1.0 cm/h with respect to measured values obtained

through laboratory tests (Hyprop device, UMS GmbH, Munich, Germany). Passing from drying to wetting conditions, K_{sw} decreases with respect to the corresponding K_{sd} (Tab. 3): in particular, the saturated hydraulic conductivity drops by half for the E horizon (3.6 cm/h than 7.2 cm/h), while this decrease is less marked for the G horizon (2.2 cm/h than 3.0 cm/h). This reconstruction shows how the G horizon has a K_s lower than the other horizons in the studied soil profile.

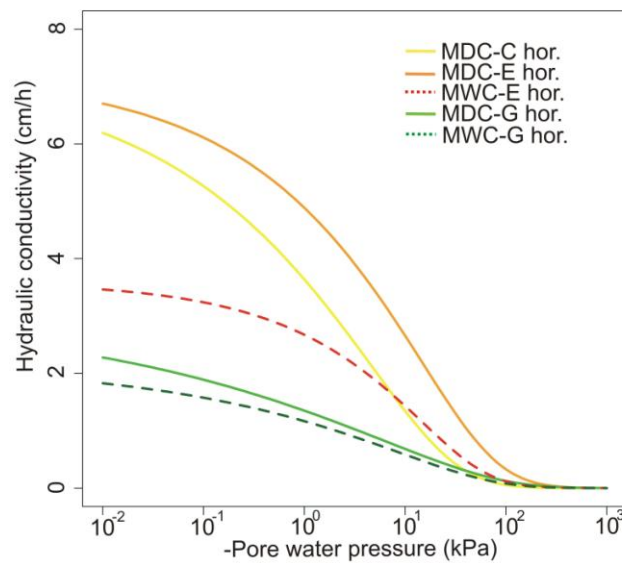


Figure 10. Modeled HCFs for studied soil horizons.

	MDC	MWC
	K_{sd} cm/h	K_{sw} cm/h
C	7.2	-
E	7.2	3.6
G	3.0	2.2

Table 3. Modeled saturated hydraulic conductivity values at pore water pressure equal to 0 kPa for the studied soil horizons.

Figure 10 shows the reconstructed curves of the hydraulic conductivity as function of the pore water pressure for both MDC and MWC cases. It can be noticed how the more evident decrease in soil hydraulic conductivity corresponds to values of pore water pressure between -10^1 and -10^2 kPa (Fig. 10). The reconstructed values of the hydraulic conductivity when the soil approaches saturated conditions are consistent with the observations on the travel time of wetting front propagation in the soil profile during rainfall events occurred in wetting periods. In fact, when the soil has a pore water pressure between 0 and -10 kPa, infiltrated rainwater travels at about 4 cm/h till 0.6 m from ground (E horizon), while, according to the curve, the hydraulic conductivity is of about 3.4 cm/h. Furthermore, in correspondence of the same pore pressure conditions, the wetting front propagates between the E and G horizons in nearly 2 cm/h, while, according to the curve, the hydraulic conductivity is of about 1.7 cm/h.

3.4 Comparison between modeled and monitored water content and pore water pressure trends

The reconstructed SWCCs and HCFs parameters have been used as input data for the HYDRUS-1D code to model the trend of soil water content (Fig. 11) and soil pore water pressure (Fig. 12) at different depths in the period between 18th January 2014 and 9th March 2014. This time span has been chosen because it comprises the period antecedent the shallow landslide, that occurred on the experimental slope between 28th February and 2nd March 2014, and the days immediately after this event. This period was characterized by many close rainfalls and a high cumulated amount of 169.8 mm in 41 days. The use of the HYDRUS-1D code aimed at modeling the pore water pressure trends for the F horizon (-1.0 m), which was not available since the monitored data in correspondence of the analyzed time span. The main goal was to compare the safety factor trends computed through the Lu and Godt's model on the basis of either the water content or the pore water pressure at -1.0m from ground level, where the shallow landslides failure surface developed on 2nd March 2014.

The modeling accounted for the hysteretic behavior of the soil horizons, by considering both the MDCs and the MWCs parameters (Tab. 2, 3). Due to the lack of SWCC and HCF parameters for the D (-0.4 m) and the F (-1.0 m) horizons, the values obtained in correspondence of the E horizon (-0.6 m) have been assigned to these levels as well. This choice is linked to the similar grain size distribution and carbonate content of these three levels (Tab. 1).

The modeled trends are in good agreement with the monitored trends for both soil water content and pore water pressure (Fig. 11, 12). RMSE values of the modeled trends (Fig. 11, 12) are rather low and this confirms the effectiveness of the reconstructed SWCCs and HCFs properties used in the modeling. The highest RMSE values were found for modeled soil water content of the F and G horizons (Fig. 11). Instead, the modeled water content at different depths in correspondence of the three days when the shallow landslide occurred (28th February- 2nd March) are very similar to the monitored ones (Fig. 11).

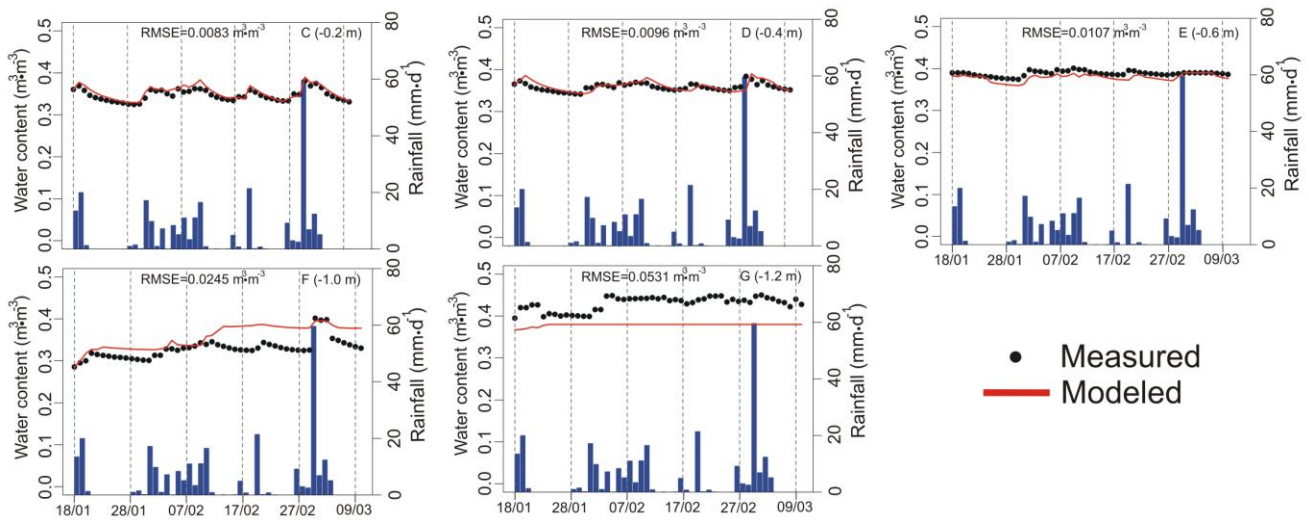


Figure 11. Comparison between measured and estimated by HYDRUS-1D code soil water content at different depths in the studied soil for the period between 18th January 2014 and 9th March 2014.

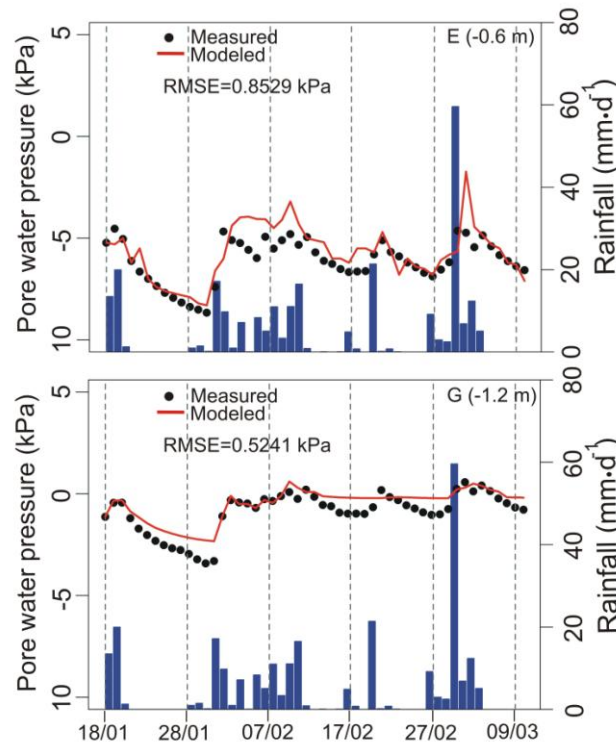


Figure 12. Comparison between measured and estimated by HYDRUS-1D code soil pore water pressure at different depths in the studied soil for the period between 18th January 2014 and 9th March 2014.

As regards the G horizon, the measured and modeled trends are parallel, even if the modeled one keeps lower of about $0.04\text{--}0.05 \text{ m}^3 \cdot \text{m}^{-3}$ (Fig. 11). The difference between measured and modeled water content could be linked to heterogeneities in this soil porosity and saturated water content with respect to the values measured through laboratory tests and SWCCs reconstruction, which are required in HYDRUS-1d for modeling.

The modeled trends of pore water pressure are in good agreement with the measured values (RMSE less than 1 kPa), in particular for the G horizon (Fig. 12). Instead, the modeled pore water pressure of the E horizon during the landslide triggering event is quite higher than the monitored values, even if, as shown by the monitoring, no positive pressures were observed (Fig. 12).

Given the reliability of modeled pore pressures at 0.6 and 1.2 m from ground level, it was decided to employ the pore water pressures modeled by HYDRUS-1d at 1.0m as input data for the safety factor computation through the Lu and Godt's model at this depth (F horizon).

3.5 Simplified slope stability analysis

The selected slope stability models (Lu and Godt's and SLIP model) have been applied to the test-site slope for the period between 18th January and 9th March 2014, during which the occurrence of a shallow landslides was observed on the same slope. The safety factor was calculated by considering a slope angle (β) equal to 30.2° and the required soil hydrological parameters (soil water content and soil pore water pressure).

The selected models required some similar soil parameters such as the soil unit weight γ , the friction angle ϕ' and the effective cohesion c' (Tab. 4, 5). Furthermore, the SLIP model required soil specific weight G_s and soil porosity p (Tab. 5). For the SLIP model application, the values of parameters A and λ were chosen on the basis of experimental results reported elsewhere (Montrasio and Valentino, 2008) for similar types of soil. The model parameter α' was considered equal to 3.4 on the basis of experimental measurements (Montrasio and Valentino, 2007). The coefficient ξ , which accounts for both runoff and leakage, is considered a constant calibration coefficient and was assumed equal to 0.7. K_T parameter value of 7.430 d⁻¹ was chosen on the basis of the saturated hydraulic conductivity K_s estimation.

The Lu and Godt's model has been applied by considering the evaluation of the required suction stress σ^s on the basis of either the water content or the pore water pressure (Eq. 4, 5), respectively. This choice is due to the intention of identifying the possible differences on modeling the slope

safety factor by taking into account water content or pore water pressure data and to investigate the role played by considering soil MDC or MWC properties in this kind of model.

The SWCC parameters for suction stress estimation were evaluated on the basis of field reconstructed hysteretic SWCCs. The properties referred to the MDC paths are indicated by the suffix d, while the ones referred to the MWC paths by the suffix w (Tab. 3).

The Lu and Godt's model was directly applied to the soil horizons where both water content and pore water pressure measurement devices are installed. In these reconstructions, the soil hydrological and geotechnical parameters effectively measured at these depths (Tab. 3) were assumed as input data. Due to the lack of field measurements at some depths (C and D horizons) and given the similarity of the main geotechnical properties (Tab. 1) in the top-soil profile, the mechanical and hydrological properties measured in the E horizon (0.6 m from ground) (Tab. 3) have been assigned to the C (0.2 m from ground) and D (0.4 m from ground) horizons as well. Moreover, for the same reason, the hydrological properties of the E horizon have been assigned to the F horizon (1.0 m from ground level). The G horizon is characterized by different hydrological features due, in particular, to its high carbonate content. Due to the break of the tensiometer, it was not possible to reconstruct the safety factor based on pore water pressure at 0.2 m from ground.

Since the SLIP model considers the soil as homogeneous along the depth, it was decided to take into account the mean values of measured γ , ϕ' , c' and p of the different layers till 1.0 m from ground (Tab. 4). On the other hand, 1.0 m is also the failure surface depth of the landslide occurred on 28th February - 2nd March 2014. The safety factor trend obtained from the SLIP model was compared with those obtained through the Lu and Godt's model on the basis of either the water content or the pore water pressure at the same depth.

Soil hor.	Depth m	β $^{\circ}$	MDC							MWC			
			γ	ϕ'	c'	θ_{sd}	α_d	θ_{rd}	n_d	θ_{sw}	α_w	θ_{rw}	n_w
			kN/m ³	$^{\circ}$	kPa	m ³ ·m ⁻³	kPa ⁻¹	m ³ ·m ⁻³	-	m ³ ·m ⁻³	kPa ⁻¹	m ³ ·m ⁻³	-
C	0.2	30.2	17.0	31.0	0.0	0.370	0.016	0.01	1.30	-	-	-	-
D	0.4		16.7	31.0	0.0	0.425	0.007	0.01	1.35	0.395	0.010	0.01	1.43
E	0.6		16.7	33.0	0.0	0.425	0.007	0.01	1.35	0.395	0.010	0.01	1.43
F	1.0		18.6	33.0	0.0	0.425	0.007	0.01	1.35	0.395	0.010	0.01	1.43
G	1.2		18.2	26.0	29.0	0.390	0.004	0.01	1.26	0.370	0.006	0.01	1.35

Table 4. Input parameters for Lu and Godt's model.

Soil hor.	Depth m	β $^{\circ}$	γ	ϕ'	c'	G_s	p	A	λ	α	ξ	K_T
			kN/m ³	$^{\circ}$	kPa	kN/m ³	-	-	-	-	-	d ⁻¹
Mean	1.0	30.2	17.7	32	0.0	27	0.46	80	0.4	3.4	0.7	7.430

Table 5. Input parameters for SLIP model.

By considering the Lu and Godt's model, the suction stress and the safety factor trends followed the hydrological parameters trends during and after rainy days. The most superficial soil levels were affected by each single rainfall event of the analyzed period, while for the F horizon at a depth of 1.0 m, the suction stress and safety factor decreased progressively with the increase of the cumulated rainfall, with a more abrupt change during the shallow landslide triggering event (Fig. 13, 14).

By considering both water content and pore water pressure the unstable condition ($F_s \leq 1$) of the failure at 1m from the ground is fairly well estimated (Fig. 13, 14). The safety factor at a depth of 1m decreases till 1 (unstable condition) when calculated on the basis of both the field measured

water content, by using MWC parameters, and the field measured pore water pressure, by using either MDC or MWC parameters.

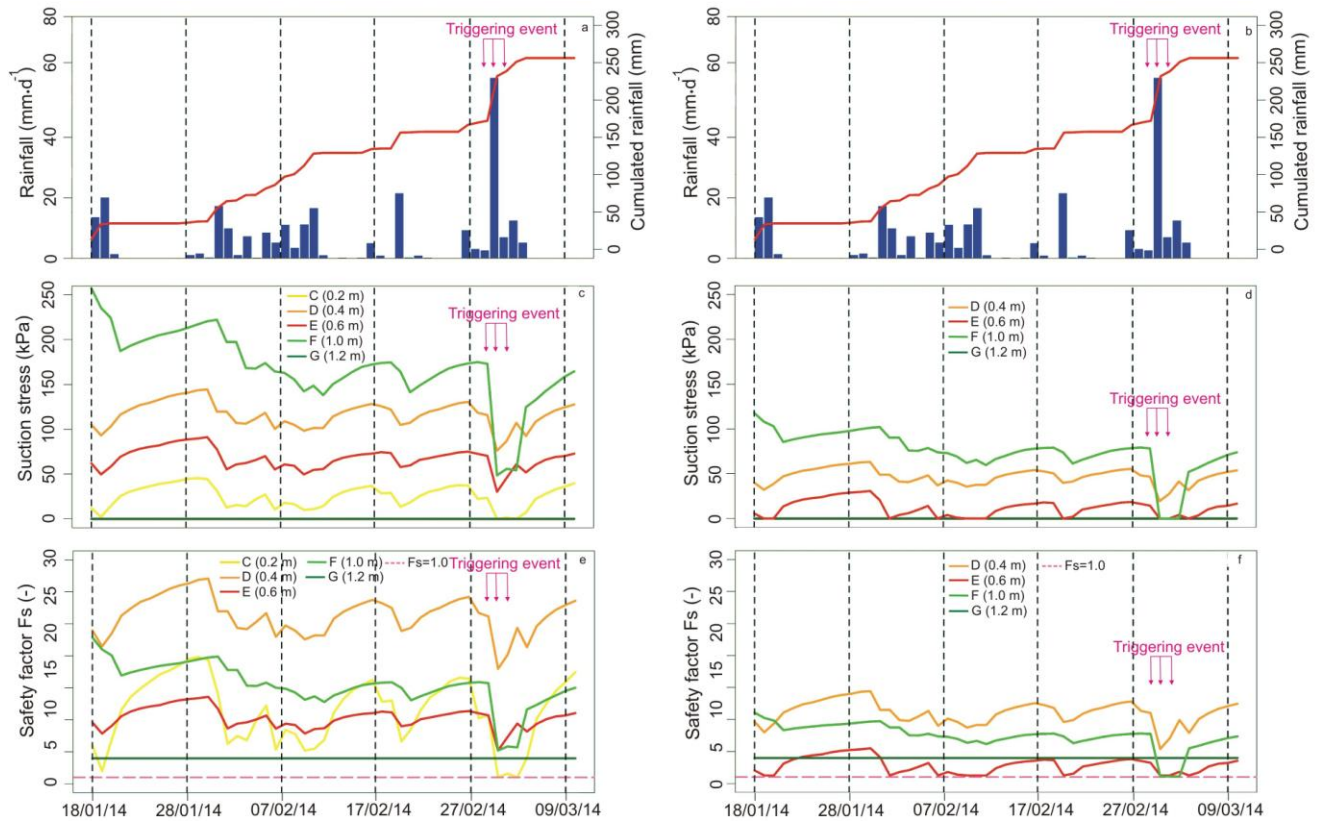


Figure 13. Safety factor trends reconstructed using Lu and Godt's model since water content data between 18th January and 9th March 2014: a, b) cumulated rainfall amount of the period; c, d) suction stress modeled using MDC or MWC properties; e, f) safety factor modeled using MDC or MWC properties.

On the contrary, the safety factor calculated on the basis of field water content by using MDC parameters keeps higher than 1 (stable condition) for the same depth all over the considered period (Fig. 13e). The triggering time is identified when suction stress decreases till 0 kPa (Fig. 13, 14). In particular, the safety factor keeps constant around 1 during the last two days of the rainfall event which triggered the landslides (1st and 2nd March), (Fig. 13, 14).

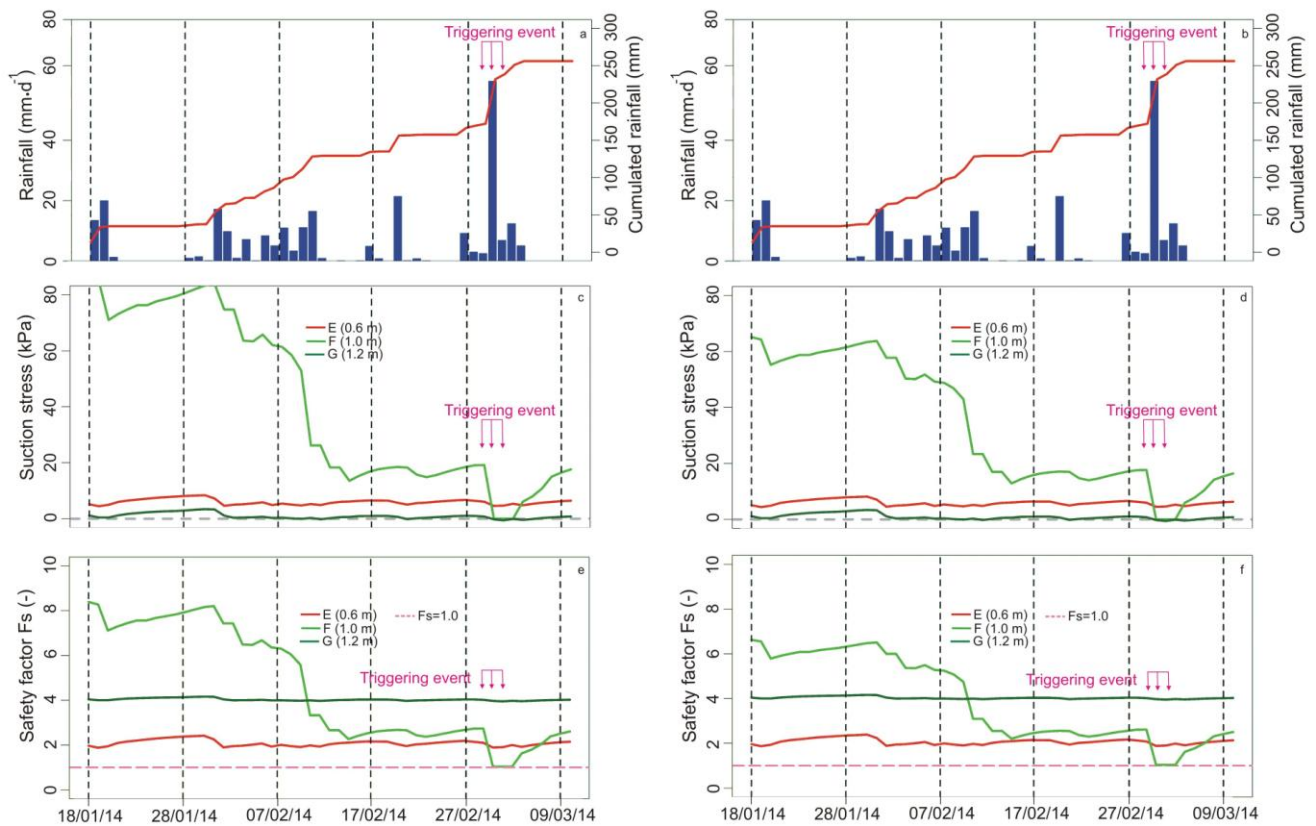


Figure 14. Safety factor trends reconstructed using Lu and Godt's model since pore water pressure data between 18th January and 9th March 2014: a, b) cumulated rainfall amount of the period; c, d) suction stress modeled using MDC or MWC properties; e, f) safety factor modeled using MDC or MWC properties.

Instead, the suction stress evaluated on the basis of the water content reached nil values also for other depths during the analyzed time span.

At 1.2 m from ground level, in the G horizon, suction stress keeps constant at 0 kPa for both MDC and MWC parameters due to the completely saturated condition of this horizon, and, as a consequence, also the modeled safety factor does not change (Fig. 13). At the same depth, the reconstructed suction stress evaluated on the basis of pore water pressure changes a little bit during

the same period, sometimes reaching negative values (about -2 kPa). As a consequence, the safety factor shows little variations linked to these changes as well (Fig. 14). In both cases the high soil cohesion (29 kPa) is enough to keep the safety factor values in the stable range ($F_s > 1$; Fig. 13, 14).

Moreover, it can be noticed that at 0.6 m from ground level suction stress estimated on the basis of field water content by using MWC parameters also decreases till 0 kPa in correspondence of different instants further than the triggering event. In correspondence of these instants, the safety factor values are slightly higher than the unstable condition ($F_s=1$) (Fig. 13d, f). By considering the reconstructions made on the basis of pore water pressure by using both MDC and MWC parameters, the suction stress does not decrease till 0 kPa, and thus the safety factor keeps in the stable range with values around 2 (Fig. 14). In agreement with these reconstructions, no shallow landslides were observed at this depth during the analyzed period.

During the triggering event, suction stress evaluated on the basis of water content data at 0.2 m also reached 0 kPa, but the safety factor keeps slightly above 1, due to the geotechnical and mechanical soil properties (Fig. 13c, e).

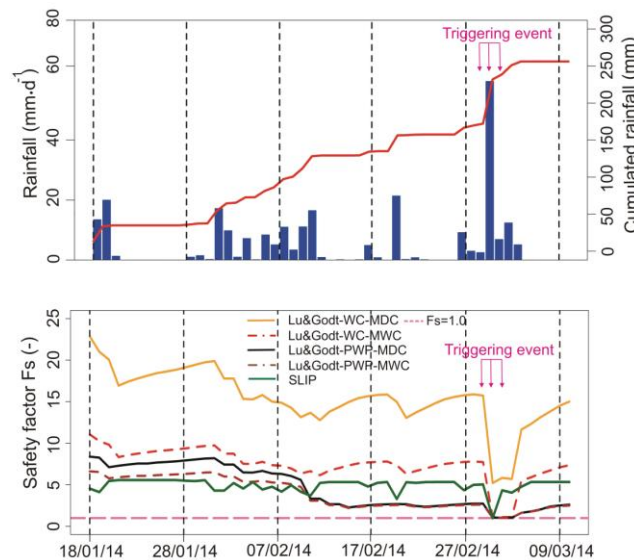


Figure 15. Comparison between safety factor trends estimation using Lu and Godt's and SLIP model between 18th January and 9th March 2014 at 1.0 m from ground.

The effect of hydrological hysteresis seems to be more marked if the suction stress and the safety factor are estimated on the basis of water content data. In fact, at the same depth, some relevant differences between the reconstructions obtained by using either MDC or MWC parameters are evident if water content data are used. The main differences can reach values in the order of 50 kPa for the suction stress and values in the order of 5 for the safety factor (Fig. 13). On the other hand, the differences given by considering or not the hysteresis in the modeling based on pore water pressure data are very limited, and are in the order of the second decimal term for both the suction stress and the safety factor when the suction stress is lower than 50 kPa, i.e. when the soil approaches saturated conditions (Fig. 14).

The slope safety factors evaluated at 1.0m from ground level by using both the Lu and Godt's model and the SLIP model have been compared (Fig. 15). The SLIP model identifies an unstable condition only in correspondence of the 1st March, when the safety factor abruptly decreases till 1.0 (Fig. 15). The trend of the safety factor reconstructed by the SLIP model seems less affected by the different rainfall events than the Lu and Godt's model estimations, with the safety factor that changes significantly only in correspondence of high rainfall amounts (Fig. 15).

4. Discussion

4.1 Shallow landslides triggering mechanism in the test-site slope

As shown in correspondence of the shallow landslide triggering event, these phenomena develop in the test-site slope in relation with the soil hydrological conditions, which are strictly linked with rainfall trends in time.

From the monitoring data it is clear that in wetting and rainy periods, in particular during winter and spring months, the studied soil profile approaches or reaches saturated conditions, with pore water pressure higher than -10^1 kPa, in the most shallow soil horizons, till about 0.6 m from ground. In the shallowest soil levels, completely saturated conditions could be reached only during the wetting front propagation, even if, given the probable non-equilibrium conditions due to this fast infiltration, the pore water pressure does not increase significantly, thus maintaining values between -5 and -3 kPa. Then the suction stress effects due to the pore water pressure are able to keep stable the soil at this level, as shown by the reconstructions of the safety factor based on this parameter (Fig. 14).

In the same wetting periods, frequent rainfall events determine a progressive infiltration of the rainwater till the deepest soil levels, leading to the formation of a perched-water table in correspondence of the less permeable soil horizon of the profile, i.e. in the calcic G horizon. The presence of this water table is testified by the fully saturated conditions and by the development of near 0 kPa or positive pore water pressure monitored in correspondence of this level. Despite of the development of positive pore water pressure and the complete reduction of suction stress effect, the high soil effective cohesion of the G horizon (29 kPa) determines that soil failures cannot form at this depth, as testified by the safety factor trends, which keep in the stable condition (safety factor between 3.5 and 4.0; Fig. 13, 14).

By analyzing the monitoring time span, during the wetting periods, particularly intense rainfall events, as those that triggered the analyzed shallow landslide, can provoke an uprising of the perched-water table till the F horizon overlying the G one, leading to the complete saturation of the soil levels at about 1.0 m from ground. From the monitored data, this uprising seems not frequent and occurs only for significant cumulated rainfall amount, as testified by the values of monitored water content at 1.0 m, which, even in wetting periods, keeps significantly lower than both the overlying levels and the underlying G horizon. As shown in Fig. 13 and 14, the uprising and the

consequent saturation of the soil at 1.0 m from ground level causes the complete reduction of the suction stress effects, and thus, linked with the nil value of the soil effective cohesion, this can lead to the development of shallow failures, represented by the safety factor values around 1.0 in Fig. 13, 14, 15.

4.2 Effects of the hydrological hysteresis on safety factor reconstruction

Modeling the safety factor through Lu and Godt's equation allows for taking into account the hydrological hysteresis, because suction stress can be reconstructed by using alternatively MDC or MWC fitting parameters of Van Genuchten equation.

Figures 13e, f and 14e, f show the effect of hydraulic hysteresis on the slope stability. The differences on the modeled safety factor trends at the same depth are linked with the differences on suction stress reconstructions, which, in their turn, are affected by SWCCs properties according to equations 4 and 5 .

Generally, suction stress evaluated on the basis of drying parameters seems to model an higher contribute to the stability than the wetting suction stress. This effect is more evident when the suction stress, and then, the safety factor, is modeled on the basis of soil water content. As shown in Fig. 16, for three soil levels where suction stress was modeled from both water content and pore pressure (E, F and G horizons), at values of soil water content close to saturation, MDC reconstructed suction stresses are at least 30 kPa higher than the corresponding wetting ones, and this difference increases with the decrease in water content.

The same difference is evident in the safety factor trend modeled on the basis of water content data (Fig. 16). In this case, at the same soil water content, safety factor in drying conditions is at least 3.0 times higher than that in wetting conditions. These results are consistent with what reported by

other authors about modeling suction stress and safety factor by considering or not the hysteretic effects (Likos et al., 2013).

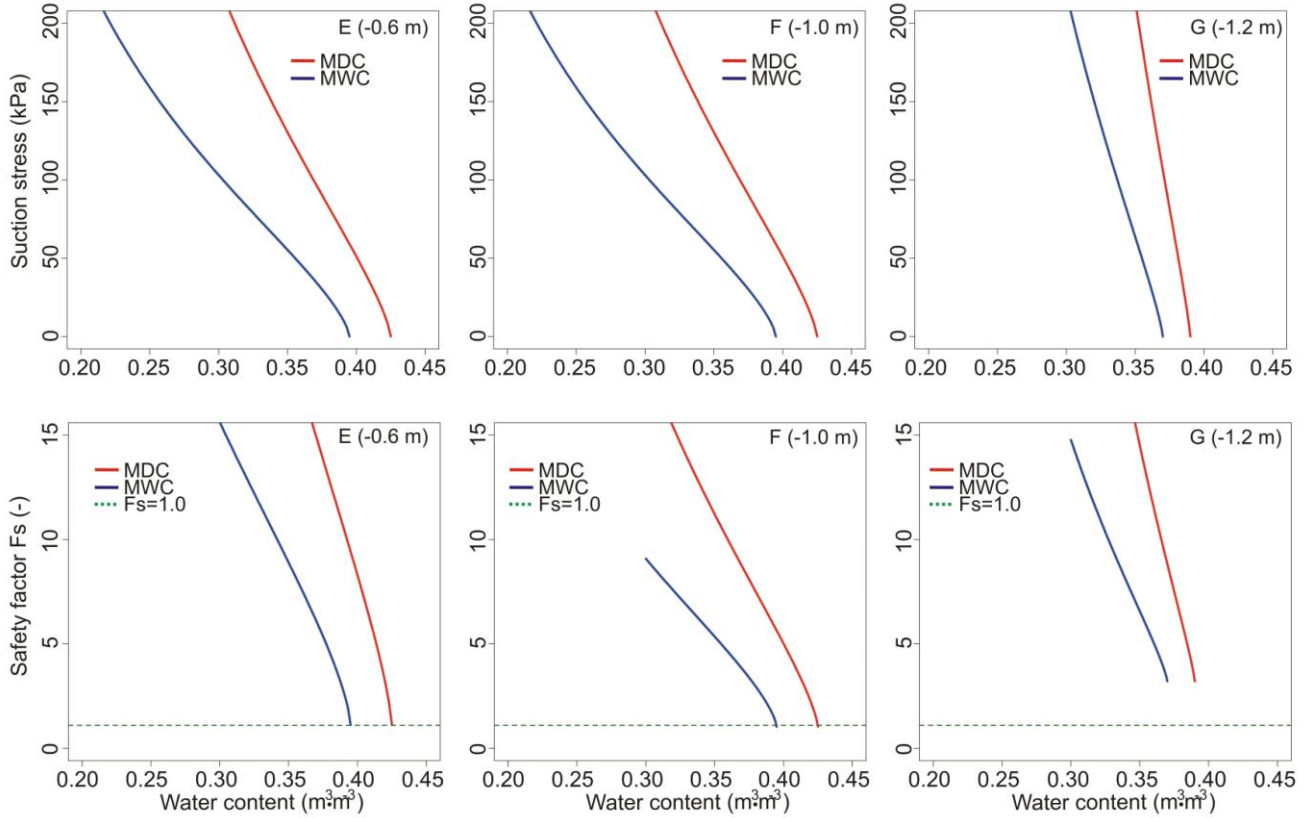


Figure 16. Suction stress and Lu and Godt's model safety factor as a function of soil water content for different soil levels of the test-site slope.

For the analyzed soil, the safety factor as a function of soil-water content decreases towards the minimum value much earlier when MWC parameters than MDC parameters are used, and the same effect is visible on the corresponding suction stress values (Fig. 16). Moreover, the suction stress and the safety factor curves do not connect at the lowest value, due to the presence of a not-closed hysteresis, with $\theta_{sw} < \theta_{sd}$.

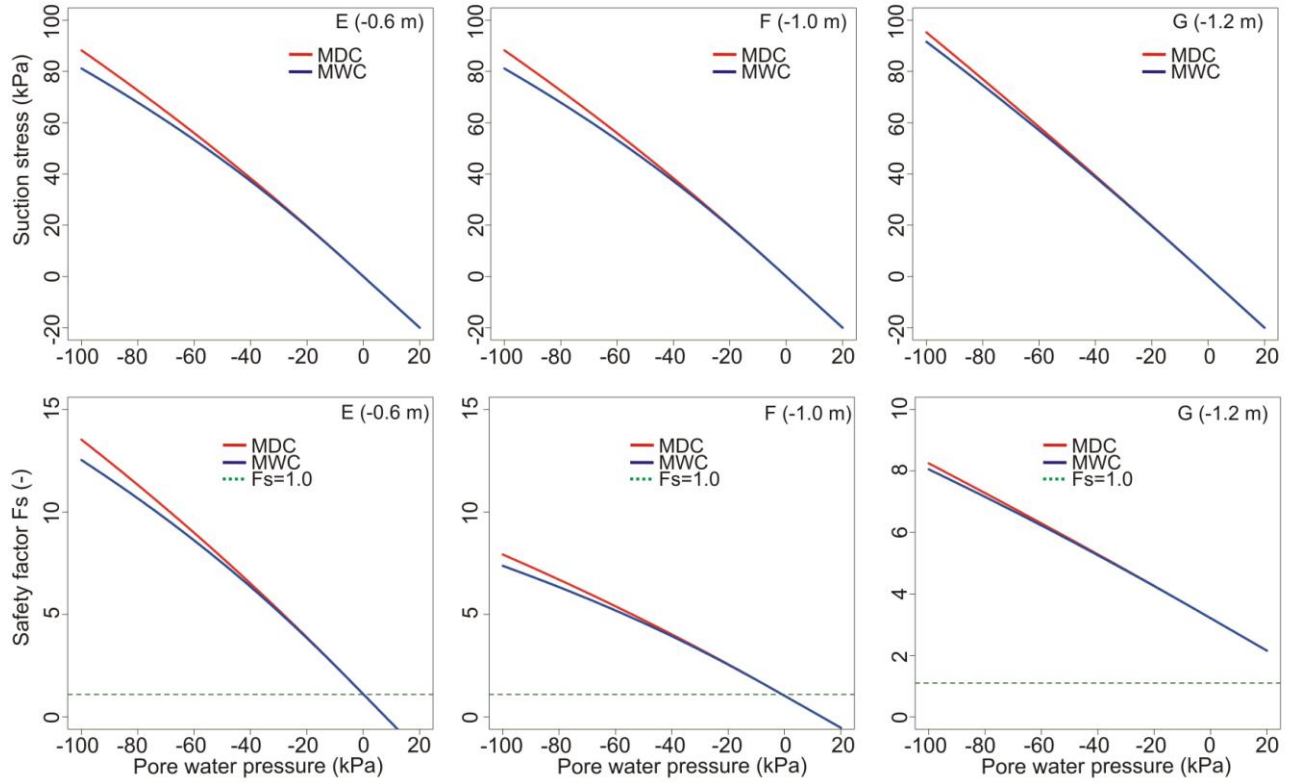


Figure 17. Suction stress and Lu and Godt's model safety factor as a function of soil pore water pressure for different soil levels of the test-site slope.

If suction stress and the corresponding safety factor are evaluated on the basis of pore water pressure, the effects of an increase of these two parameters by taking into account the MDC properties with respect to the MWC ones are still present, but they are less evident (Fig. 17). In fact, by considering a pore water pressure value equal to -100 kPa, the differences are in the order of less than 10 kPa for suction stress and less than 2.0 for the safety factor, respectively. These gaps decrease with pore water pressure increase, till a complete convergence of the curves when pore water pressure reaches nil and then positive values (Fig. 17). This different behaviour with respect to modeling based on water content is linked to the different formulations of suction stress estimation. In fact, for estimating suction stress starting from pore pressure (Eq. 5) the saturated water content θ_s is not taken into account as in the equation containing water content (Eq. 4).

It is important noting that, while the estimated suction stress based on water content, according to Eq. 4, can reach values till 0 kPa, suction stress based on pore water pressure can continue to decrease in presence of positive pore water pressure (Eq. 5). For this reason, the safety factor estimated starting from pore water pressure can continue to decrease in presence of positive pressure (Fig. 17), while the safety factor evaluated on the basis of the water content reaches a minimum constant value for soil water content equal to θ_s .

4.3 Effects of considering water content or pore water pressure on safety factor

The three selected models (Lu and Godt based on water content, Lu and Godt based on pore water pressure and SLIP) allowed for correctly estimating the triggering conditions of a shallow landslide in the studied slope (Fig. 13, 14, 15). By considering Lu and Godt's model based on water content, the correct estimation using wetting parameters, instead of the drying parameters, is consistent with the fact that when shallow failure develops, the soil is affected by an infiltration, thus the wetting parameters are more suitable than the drying ones. These differences are not so evident when the safety factor is calculated through Lu and Godt's model based on pore water pressure. Instead, in the case of a more marked hysteresis with a higher gap between MDC and MWC than the considered soils, the distance between the two modeled safety factors could increase also when the pore water pressure is close to 0 kPa.

When soil water content data are considered in both Lu and Godt's and SLIP models, the minimum values of the safety factor is reached at complete saturation ($\theta = \theta_s$), and then the safety factor cannot decrease further. Modeling the safety factor on the basis of water content can make a correct prediction of the sliding only when a shallow landslide develops in unsaturated conditions or for θ equal to θ_s , so that pore water pressure is less or equal to 0 kPa.

Instead, the safety factor based on pore water pressure allows for taking into account also positive pore water pressures. When the safety factor is slightly higher than 1, $\theta = \theta_s$ and pore water pressure is equal to 0 kPa, as in the case of the E horizon ($F_S=1.1$), the development of positive pore water pressures could get the slope unstable (safety factor less than 1), as shown in Fig. 17. For this reason, a correct prediction can be made only if the safety factor is modeled considering the pore water pressure, especially in situations in which the shallow failures develop not immediately when the soil reaches saturation but only after the development of positive pressures (Lim et al., 1996; Wang and Sassa, 2001; Leung and Ng, 2013). In this condition, the modeling of safety factor based on water content can only indicate conditions which can lead to shallow landslides triggering, without a correct prediction of the failure instant.

5. Conclusions

An analysis of water content and pore water pressure effects on modeling shallow landslides safety factor at slope scale through different models has been performed. The test-site slope was monitored continuously in time with a field station to investigate the soil hydrological responses in time, by measuring soil water content and pore water pressure trends required for the safety factor estimations.

During the monitoring phase, the studied slope experienced a shallow landslide event due to intense rainfalls. The triggering mechanism of this phenomenon was described by analyzing the field data collected during the event. The conditions leading to shallow failures develop in wetting periods, especially in winter and spring, when very frequent rainfalls cause an increase in soil water content and a corresponding decrease in pore water pressure till values close to 0 kPa in the whole soil profile. In these periods, in correspondence of the less permeable horizon in the soil profile, a perched water table forms and can rise up in consequence of very intense rainfalls till about 1 m from ground. At this depth, the uprising of the water table get saturated conditions and leads to an

increase of pore water pressure even slightly over a nil value, which, linked with the nil effective soil cohesion, allows for the shallow landslides mechanism.

The monitored data allowed for the field reconstruction of hysteretic SWCCs and HCFs of the monitored soils and the estimation of MDCs and MWCs parameters. These parameters have been used to apply the Lu and Godt's model in order to investigate the effect of considering either drying or wetting parameters on safety factor evaluation.

The safety factor trends obtained by different models correctly predicted unstable conditions ($F_s \leq 1$) in correspondence of the really occurred shallow landslide at 1 m from ground, on the basis of both water content and pore water pressure data. In particular, a better prediction through Lu and Godt's model gets when the safety factor, especially if based on the soil water content, is modeled considering the hydrological hysteresis effects, which affect the studied soils during the infiltration phase.

Modeling the safety factor on the basis of water content can make a correct prediction of the failure only when a shallow landslide develops in unsaturated conditions or in conditions of θ equal to θ_s , so that pore water pressure is less or equal to 0 kPa. Instead, when the triggering mechanism is linked with the development of positive pore water pressures, a correct prediction can be made only if the safety factor is modeled considering the pore water pressure. In this condition, the modeling of safety factor based on water content can only indicate conditions which can lead to shallow landslides triggering, without a correct prediction of the instant of failure mechanism.

Further developments will be linked to the application of the considered models (Lu and Godt's and SLIP models) at both local and regional scale, also to better understand the difference on shallow landslides triggering prediction considering water content or pore water pressure data.

Acknowledgments

We thank Dr. M.A. Leoni of the Riccagioia S.C.P.A. - Centro di Ricerca Formazione e Servizi della Vite e del Vino for the pedological analysis of the soil of the experimental site. We also thank Dr. M. Setti and Dr. L. Marinoni for the mineralogical analysis of the levels of the test-site slope soil profile and the Ditta Rossi s.r.l. (Brescia, Italy) for the acquisition of the aerial photographs of the study area. Moreover, we acknowledge Dr. A. Wayllace, Dr. B. Ebel and Dr. J.W. Godt for some constructive considerations during the phase of preparation and writing of the work.

The authors wish to thank the anonymous reviewers for their suggestions and contribution to the work.

References

Askarinejad A, Casini F, Bischof P, Beck A, Springman SM (2012) Rainfall induced instabilities: a field experiment on a silty sand slope in northern Switzerland. *Riv It Geot* 3:50-71

Bathurst JC, Moretti G, El-Hames A, Moaven-Hashemi A, Burton A (2005) Scenario modelling of basin-scale, shallow landslide sediment yield, Valsassina, Italian Southern Alps. *Nat Haz Earth Sys Sci* 5:189-202

Baum RL, Godt JW, Savage WZ (2010) Estimating the timing and location of shallow rainfall-induced landslides using a model for transient, unsaturated infiltration. *Jour Geoph Res.* doi:10.1029/2009JF001321

Baum RL, Savage WZ, Godt, JW (2002) TRIGRS--A FORTRAN Program for Transient Rainfall Infiltration and Grid-Based Regional Slope-Stability Analysis: U.S. Geological Survey Open-File Report 02-0424, 35 pp, 2 appendices

Baumhardt RL, Lascano RJ (1993) Physical and hydraulic properties of a calcic horizon. *Soil Sci* 155:368-375

- Bittelli M, Flury M (2008) Errors in water retention curves determined with pressure plates. *Soil Sci Soc Am J* 73:1453-1460. doi:10.2136/sssaj2008.0082
- Bittelli M, Salvatorelli F., Rossi Pisa P (2008). Correction of TDR-based soil water content measurements in conductive soils. *Geoderma* 143: 133-142
- Bittelli M, Valentino R, Salvatorelli F., Rossi Pisa P (2012) Monitoring soil-water and displacement conditions leading to landslide occurrence in partially saturated clays. *Geomorphology* 173-174:161-173. doi:10.1016/j.geomorph.2012.06.006
- Caine N (1980) The rainfall intensity-duration control of shallow landslides and debris flow. *Geogr Ann A* 62:23–27
- Campbell GS, Gee GW (1986) Water potential: Miscellaneous methods. In: A Klute (ed) *Methods of soil analysis Part 1 Physical and mineralogical methods*, 2nd edn., Agron. Monogr. 9. ASA and SSSA, Madison, WI, pp 619- 632
- Campbell RH (1975) Soil Slips, Debris Flows and Rainstorms in the Santa Monica Mountains and Vicinity, Southern California. Geological Survey Professional Paper 851, 51 pp
- Cancelli A, Nova R (1985) Landslides in soil debris cover triggered by rainstorms in Valtellina (central Alps – Italy). In: *Proceedings of the 4th International Conference and Field Workshop on Landslides*, The Japan Geological Society, Tokyo, pp 267–272
- Capra L, Lugo-Hubp J, Borselli L (2003) Mass movements in tropical volcanic terrains: the case of Teziùtlan (Mexico). *Eng Geol* 69:359-79. doi:10.1016/S0013-7952(03)00071-1
- Cascini L, Cuomo S, Guida D (2008) Typical source areas of May 1998 flow-like mass movements in the Campania region, Southern Italy. *Eng Geo* 96:107-125. doi:10.1016/j.enggeo.2007.10.003

- Cevasco A, Brandolini P, Scopesi C, Rellini I (2013) Relationships between geo-hydrological processes induced by heavy rainfall and land use: the case of 25 October 2011 in the Vernazza catchment (Cinque Terre, NW Italy). *J Maps* 9, 2:289-298
- Cuomo S, Della Sala M (2013) Rainfall-induced infiltration, runoff and failure in steep unsaturated shallow soil deposits. *Eng Geol* 162:118-127. doi:10.1016/j.enggeo.2013.05.010
- Cruden DM, Varnes DJ (1996) Landslide types and processes. In: Turner AK, Schuster RL (eds) *Landslides: investigation and mitigation Sp. Rep. 247*, Transportation Research Board, National Research Council, National Academy Press, Washington DC, pp 36-75
- D'Amato Avanzi G, Galanti Y, Giannecchini R, Lo Presti D, Puccinelli A (2013) Estimation of soil properties of shallow landslide source areas by dynamic penetration tests: first outcomes from Northern Tuscany (Italy). *Bull Eng Geol Environ* 72:609-624. doi:10.1007/s10064-013-0535-y
- Damiano E, Olivares L, Picarelli L (2012) Steep-slope monitoring in unsaturated pyroclastic soils. *Eng Geol* 137-138:1-12. doi:10.1016/j.enggeo.2012.03.002
- Diamantopoulos E, Iden SC, Durner W (2012) Inverse modelling of dynamic nonequilibrium in water flow with an effective approach. *Water Resources Research* 48, 3. doi: 10.1029/2011WR010717
- Ebel BA, Loague K, Borja RI (2010) The impacts of hysteresis on variably saturated hydrologic response and slope failure. *Environ Earth Sci* 61:1215-1225. doi:10.1007/s12665-009-0445-2
- Eichenberger J, Ferrari A, Laloui L (2013). Early warning thresholds for partially saturated slopes in volcanic ashes. *Computers Geotech* 49:79-89. doi:10.1016/j.compgeo.2012.11.002

- Flint AL, Campbell GS, Ellett KM, Calissendorf C (2002) Calibration and temperature correction of heat dissipation matric potential sensors. *Soil Sci Soc Am J*, 66:1439-1445. doi:10.2136/sssaj2002.1439
- Fredlund DG, Morgestern NR, Widger RA (1978) The shear strength of unsaturated soils. *Can Geotech J* 15:313-321
- Fredlund DG, Xing A, Fredlund M D, Barbour SL (1996) The relationship of the unsaturated soil shear strength to the soil water characteristic curve. *Can Geotech J*, 33, 3:440-448
- Fredlund DG, Sheng D, Zhao J (2011) Estimation of soil suction from the soil-water characteristic curve. *Can Geotech J* 48:186-198. doi:10.1139/T10-060
- Fuchu D, Lee CF, Sijing W (1999) Analysis of rainstorm-induced slide-debris flows on a natural terrain of Lantau Island, Hong Kong. *Eng Geol* 51:279-90. doi:10.1016/S0013-7952(98)00047-7
- Gardner WR (1958) Some steady-state solutions of the unsaturated moisture flow equation with application to evaporation from a water table. *Soil Sci* 85:228-232
- Gee GW, Ward AL, Zhang ZF, Campbell GS, Mathison, J (2002) The influence of hydraulic nonequilibrium on pressure plate data. *Vadose Zone Journal* 1:172-178. doi: 10.2113/1.1.172
- Godt JW, Baum RL, Lu N (2009) Landsliding in partially saturated materials. *Geoph Res Lett* 36. doi:10.1029/2008GL03599
- Godt JW, Baum RL, Savage WZ, Salciarini D, Schulz WH, Harp EL (2008a) Transient deterministic shallow landslide modelling: Requirements for susceptibility and hazard assessment in a GIS framework. *Eng Geol* 102:214-226. doi:10.1016/j.enggeo.2008.03.019

- Godt JW, Schulz WH, Baum RL, Savage WZ (2008b) Modelling rainfall conditions for shallow landsliding in Seattle, Washington. In: Baum R.L, Godt JW, High land LM (eds.) Landslides and Engineering Geology of the Seattle, Washington, area. Geol Soc Am Rev Eng Geol 20:137-152
- Grelle G, Soriano M, Revellino P, Guerriero L, Anderson MG, Diambra A, Fiorillo F, Esposito L, Diodato N, Guadagno FM (2014) Space-time prediction of rainfall-induced shallow landslides through a combined probabilistic/deterministic approach, optimized for initial water table conditions. Bull Eng Geol Environ. doi:10.1007/s10064-013-0546-8
- Grimaldi S, Nardi F, Di Benedetto F, Istanbuluoglu E, Bras RL (2007) A physically-based method for removing pits in digital elevation models. Adv Water Resour 30:2151-2158. doi:10.1016/j.advwatres.2006.11.016
- Guzzetti F, Peruccacci S, Rossi M, Stark CP (2008) The rainfall intensity-duration control of shallow landslides and debris flows: an update. Landslides 5, 1:3–17. doi:10.1007/s10346-007-0112-1
- Harp EL, Reid ME, McKenna JP, Michael JA (2009) Mapping of hazard from rainfall triggered landslides in developing countries: examples from Honduras and Micronesia. Eng Geol 104:295-311. doi:10.1016/j.enggeo.2008.11.010
- Howard TR, Baldwin JE, Donley HE (1988) Landslides in Pacifica California, caused by the Storm. In: Landslides, Floods and Marine Effects of the Storm of January 3-5 1982 in the San Francisco Bay Region, California In: SD Ellen, GF Wieckzoreck (eds), - U.S. Geological Survey Professional Paper 1434
- IUSS Working Group WRB (2007) World Reference for Soil Resources 2006, first update 2007. FAO, Rome

- Iverson RM (2000) Landslide triggering by rain infiltration, *Water Resour Res* 36:1897-1910. doi:10.1029/2000WR900090
- Kool JB, Parker JC (1987) Development and evaluation of closed-form expressions for hysteretic soil hydraulic properties. *Water Resour Res* 23, 1:105-114. doi:10.1029/WR023i001p00105
- Lee ML, Gofar N, Rahardjo H (2009) A simple model for preliminary evaluation of rainfall-induced slope instability. *Eng Geol* 108:272-285. doi:10.1016/j.enggeo.2009.06.011
- Lehmann P, Or D (2012) Hydromechanical triggering of landslides: From progressive local failures to mass release. *Water Resour Res* 48. doi:10.1029/2011WR010947
- Leroueil S, Vaughan PR (1990) The general and congruent effects of structure of natural soils and weak rocks. *Geotechnique* 40, 467-488. doi:10.1680/geot.1990.40.3.467
- Leung AK, Ng CWW (2013) Seasonal movement and groundwater flow mechanism in an unsaturated saprolitic hillslope. *Landslides* 10,455-467. doi:10.1007/s10346-012-0343-7
- Li AG, Yue ZQ, Tham LG, Lee CF, Law KT (2005) Field-monitored variations of soil moisture and matric suction in a saprolite slope. *Can Geotech J* 42:13-26. doi:10.1139/t04-069
- Li WC, Lee LM, Cai H, Li HJ, Dai FC, Wang ML, (2013) Combined roles of saturated permeability and rainfall characteristics on surficial failure of homogeneous soil slope. *Eng Geol* 153:105-113. doi:10.1016/j.enggeo.2012.11.017
- Likos WJ, Lu N, Godt JW (2013). Hysteresis and uncertainty in soil-water retention curve parameters. *J Geotech Geoenviron Eng* 140,4. doi:10.1061/(ASCE)GT.1943-5606.0001071
- Lim TT, Rahardjo H, Chang MF, Fredlund, DG (1996) Effect of rainfall on matric suctions in a residual soil slope. *Can Geotech J* 33:618-628. doi:10.1139/t96-087

- Lu N, Godt J (2008) Infinite slope stability under steady unsaturated seepage conditions. *Water Resour Res* 44. doi:10.1029/2008WR006976
- Lu N, Godt JW (2013) Hillslope hydrology and stability. Cambridge University Press, Cambridge, U.K.
- Lu N, Likos WJ (2004) *Unsaturated Soil Mechanics*. Wiley, Hoboken, N. J.
- Lu N, Likos WJ (2006) Suction stress characteristic curve for unsaturated soil. *J Geotech Geoenviron Eng* 132:131-142. doi:10.1061/(ASCE)1090-0241(2006)132:2(131)
- Lu N, Wu B, Tan CP (2007) Tensile strength characteristics of unsaturated sands. *J Geotech Geoenviron Eng* 133:144-154. doi:10.1061/(ASCE)1090-0241(2007)133:2(144)
- Lu N, Godt JW, Wu DT (2010) A closed-form equation for effective stress in unsaturated soil. *Water Resour Res* 46. doi:/10.1029/2009WR008646
- Lu N, Kaya M, Collins BD, Godt JW (2013) Hysteresis of unsaturated hydromechanical properties of a silty soil. *J Geotech Geoenviron Eng* 139:507-510. doi:10.1061/(ASCE)GT.1943-5606.0000786
- Ma KC, Lin YJ, Maa SY, Tan YC (2012) Evaluation of the effect of hysteretic flow and root system on shallow landslide. *Soil Res* 50, 7:616-624. doi:10.1071/SR12104
- Marquardt DW (1963) An algorithm for least-squares estimation of non-linear parameters. *SIAM J Appl Math* 11:431–441.
- Martelloni G, Segoni S, Fanti R, Catani F (2012) Rainfall thresholds for the forecasting of landslide occurrence at regional scale. *Landslides* 9:485-495. doi: 10.1007/s10346-011-0308-2

- Matsushi Y, Hattanji T, Matsukura Y (2006) Mechanisms of shallow landslides on soil-mantled hillslopes with permeable and impermeable bedrocks in the Boso Peninsula, Japan. *Geomorphology* 76:92- 108. doi:10.1016/j.geomorph.2005.10.003
- Matsushi, Y, Matsukura Y (2007) Rainfall thresholds for shallow landsliding derived from pressure-head monitoring: cases with permeable and impermeable bedrocks in Boso Peninsula, Japan. *Earth Surf Process Landf* 32:1308-1322. doi:10.1002/esp.1491
- Montgomery DR, Dietrich WE (1994) A physically based model for the topographic control on shallow landsliding. *Water Resour Res* 30, 4:1153-1171. doi:10.1029/93WR02979
- Montrasio L (2000) Stability analysis of soil slip. in: Brebbia CA (ed) *Proceedings of International Conf. "Risk 2000"*, Wit Press, Southampton, pp 357-366
- Montrasio L, Valentino R (2007) Experimental analysis and modeling of shallow landslides, *Landslides* 4:291-296. doi:10.1007/s10346-007-0082-3
- Montrasio L, Valentino R (2008) A model for triggering mechanisms of shallow landslides. *Nat Haz Earth Sys Sci* 8:1149-1159. doi:10.5194/nhess-8-1149-2008
- Montrasio L, Valentino R, Losi GL (2011) Towards a real-time susceptibility assessment of rainfall-induced shallow landslides on a regional scale. *Nat Haz Earth Sys Sci* 11:1927-1947. doi:10.5194/nhess-11-1927-2011
- Montrasio L, Valentino R, Losi, GL (2012) Shallow landslides triggered by rainfalls: modeling of some case histories in the Reggiano Apennine (Emilia Romagna Region, Northern Italy). *Nat Haz* 60: 1231-1254. doi:10.1007/s11069-011-9906-5
- Mualem Y (1976) A new model predicting the hydraulic conductivity of unsaturated porous media. *Water Resour Res* 12:513-522. doi:10.1029/WR012i003p00513

- Parlange JY (1976) Capillary hysteresis and relationship between drying and wetting curves. *Water Resour Res* 12:224-228. doi:10.1029/WR012i002p00224
- Park DW, Nikhil NV, Lee SR (2013) Landslide and debris flow susceptibility zonation using TRIGRS for the 2011 Seoul landslide event. *Nat Haz Earth Sys Sci* 13:2833-2849. doi:10.5194/nhess-13-2833-2013
- Reichenbach P, Cardinali M, De Vita P, Guzzetti F (1998) Regional hydrological thresholds for landslides and floods in the Tiber River Basin (central Italy). *Environm Geol* 35, 2–3:146–159. doi:10.1007/s002540050301
- Rogers JS, Klute A (1971) The hydraulic conductivity-water content relationship during nonsteady flow through a sand column. *Soil Sci Soc Am J* 35, 5:695-700. doi:10.2136/sssaj1971.03615995003500050021x
- Ross P, Smettem KRJ (2000) A simple treatment of physical nonequilibrium water flow in soil. *Soil Sci Soc Am J* 64:1926-1930. doi:10.2136/sssaj2000.6461926x
- Rossetti R, Ottone C (1979) Esame preliminare delle condizioni pluviometriche dell'Oltrepò Pavese e dei valori critici delle precipitazioni in relazione ai fenomeni di dissesto franoso. *Geol App Idrogeol* 24, 3:83-99
- Schindler U, Müller L (2006) Simplifying the evaporation method for quantifying soil hydraulic properties. *J Plant Nutr Soil Sci* 169, 5:623-629. doi:10.1002/jpln.2005218
- Schindler U (1980) Ein schnellverfahren zur messung der wasserleitfähigkeit im teilgesättigten boden an stechzylinderproben. *Arch Acker- Pflanzenbau Bodenkd* 24:1-7

- Schmidt KM, Roering JJ, Stock JD, Dietrich WE, Montgomery DR, Schaub T (2001) The variability of root cohesion as an influence on shallow landslide susceptibility in the Oregon Coast Range. *Can Geotech J*, 38:995-1024. doi:10.1139/cgj-38-5-995
- Simoni A, Berti M, Generali M, Elmi C, Ghirotti M, (2004) Preliminary result from pore pressure monitoring on an unstable clay slope. *Eng Geol* 73:117- 128. doi:10.1016/j.enggeo.2003.12.004
- Simunek J, Jarvisb NJ, Van Genuchten MT, Gardenas A (2003) Review and comparison of models for describing non-equilibrium and preferential flow and transport in the vadose zone. *J Hydrol* 272:14-35
- Simunek J, Van Genuchten MT, Sejna M (2008) Development and applications of the HYDRUS and STANMOD software packages and realated codes. *Vadose Zone Journal*, 7:587-600. doi:10.2136/vzj2007.0077
- Simunek J, Sejna M, Saito H, Sakai M, Van Genuchten MT (2013) The HYDRUS-1D software package for simulating the movement of water, heat, and multiple solutes in variably saturated media, Version 4.16. *HYDRUS Software Series 3*, Department of Environmental Sciences, University of California Riverside, Riverside, California, USA, pp. 340
- Smethurst JA, Clarke, D, Powrie D (2012) Factors controlling the seasonal variation in soil water content and pore water pressures within a lightly vegetated clay slope. *Geotechnique* 62, 5:429-446. doi:10.1680/geot.10.P.097
- Sorbino G, Nicotera MV (2013) Unsaturated soil mechanics in rainfall-induced flow landslides. *Eng Geol* 165, 105-132. doi:10.1016/j.enggeo.2012.10.008
- Springman SM, Thielen A, Kienzler P, Friedel S (2013) A long-term field study for the investigation of rainfall-induced landslides. *Geotechnique* 14:1177-1193. doi:10.1680/geot.11.P.142

- Stakman WP, Bishay BG (1976) Moisture retention and plasticity of highly calcareous soils. *Neth J Agric Sci* 24:43-57
- Tiranti D, Rabuffetti D (2010) Estimation of rainfall thresholds triggering shallow landslides for an 24 operational warning system implementation. *Landslides* 7:471-481. doi:10.1007/s10346-010-0198-8
- Tohari A, Nishigaki M, Komatsu M (2007) Laboratory rainfall-induced slope failure with moisture content measurement. *J Geotech Geoenv Eng* 133, 5:575-587. doi:10.1061/(ASCE)J090-0241(2007)133:5(575)
- Topp GC, Miller EE (1966) Hysteresis moisture characteristics and hydraulic conductivities for glassbead media. *Soil Sci Am Proc* 30:156-162. doi:10.2136/sssaj1966.03615995003000020008x
- Topp GC, Annan JL, Davis AP (1980) Electromagnetic determination of soil water content: measurements in coaxial transmission lines. *Water Resour Res* 16:574-582. doi:10.1029/WR016i003p00574
- Tsai TL (2010) Influences of soil water characteristic curve on rainfall-induced shallow landslides. *Environ Earth Sci.* 64,2: 449-459. doi:10.1007/s12665-010-0868-9
- Van Genuchten MT (1980) A closed-form equation for predicting the hydraulic conductivity of unsaturated soils. *Soil Sci Soc Am J* 44:892-898. doi:10.2136/sssaj1980.03615995004400050002x
- Van Genuchten MT, Leij FJ, Yates SR (1991) The RETC Code for Quantifying the Hydraulic Functions of Unsaturated Soils, Version 1.0. EPA Report 600/2-91/065, U.S. Salinity Laboratory, USDA, ARS, Riverside, California
- Vanapalli SK, Fredlund DG, Pufahl DE, Clifton AW (1996) Model for the prediction of shear strength with respect to soil suction. *Can Geotech J* 33:379-392. doi:10.1139/t96-060

- Vercesi P, Scagni G (1984) Osservazioni sui depositi conglomeratici dello sperone collinare di Stradella. *Rend Soc Geol It* 7:23-26
- Vogel HJ, Weller U, Ippisch O (2010) Non-equilibrium in soil hydraulic modelling. *J Hydrol* 393:20-28. doi:10.1016/j.jhydrol.2010.03.018
- Von Ruette J, Papritz A, Lehmann P, Rickli C, Or D (2011) Spatial statistical modelling of shallow landslides-Validating predictions for different landslide inventories and rainfall events. *Geomorphology* 133:11-22. doi:10.1016/j.geomorph.2011.06.010
- Wang G, Sassa K (2001) Factors affecting rainfall-induced flowslides in laboratory flume tests *Geotechnique* 51, 7:587–599. doi:10.1680/geot.2001.51.7.587
- Wheeler SJ, Sharma RJ, Buisson MSR (2003) Coupling of hydraulic hysteresis and stress-strain behavior in unsaturated soils. *Geotechnique* 53, 1:43-54. doi:10.1680/geot.2003.53.1.41
- Wilson R.C., Wieczorek GF (1995) Rainfall thresholds for the initiation of debris flow at La Honda, California. *Environ Eng Geosci* 1, 1:11–27
- Zhan TLT, Ng CWW, Fredlund DG (2006) Instrumentation of an unsaturated expansive soil slope. *Geotech Test J* 30, 2:1-11. doi:10.1520/GTJ12704
- Zizioli D, Meisina C, Valentino R, Montrasio L (2013) Comparison between different approaches to modelling shallow landslide susceptibility: a case history in Oltrepò Pavese, Northern Italy. *Nat Haz Earth Sys Sci* 13:559-573. doi:10.5194/nhess-13-559-2013
- Zizioli D, Meisina C, Bordoni M, Zucca F (2014) Rainfall-triggered shallow landslides mapping through Pleiades images. In: Sassa K, Canuti P, Yin Y (eds) *Landslide science for a safer geoenvironment*, vol. 2, pp 325-329

Highlights

- Shallow landslides triggering mechanism was identified through field monitoring.
- Test-site slope safety factor was modelled since monitored data.
- Triggering moment was predicted since soil water content or pore water pressure.
- Soil water content safety factor gets better considering the hydrological hysteresis.
- Triggering conditions linked to positive pore water pressure cannot be identified since only soil water content.